

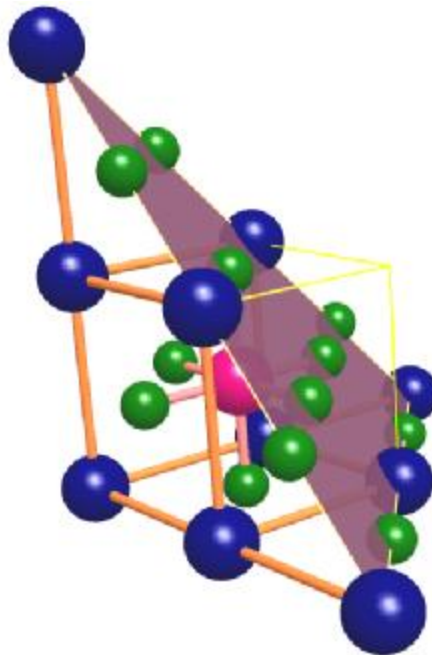
Growth and characterization of CaTiO_3 thin films with (111) orientation

Master thesis

Xin Wan

Enschede, 3rd April 2008

Major subject: Chemical Engineering



Abstract

In this thesis, epitaxial growth of CaTiO_3 thin film along (111) orientation on LaAlO_3 substrates with Pulsed Laser Deposition is discussed. Density Functional Theory Calculations have shown the existence of a ferroelectric phase in CaTiO_3 . This phase can be stabilized by growing CaTiO_3 with compressive strain in the (111) direction. Therefore (111) LaAlO_3 substrates were chosen. Thermal annealing and alkaline etching were used to produce single terminated substrates with smooth step edges. X-ray diffraction and transmission electron microscope measurements show the coherent growth of CaTiO_3 thin film. Electrical measurements were done on films that have CaRuO_3 bottom and top electrodes. However the electrical measurements showed no signal of ferroelectricity at room temperature.

Contents

Abstract.....	3
Chapter 1. Introduction	6
1.1 Ferroelectricity	6
1.2 Ferroelectric phase in CaTiO_3 by epitaxial strain	8
1.3 Outline	10
Chapter 2. Fabrication and analysis tools	12
2.1 Principle of the pulsed laser deposition	12
2.2 Reflection high-energy electron diffraction	13
2.3 Atomic force microscopy	14
2.4 X-ray diffraction	15
2.5 High resolution transmission electron microscopy	16
Chapter 3. Surface treatment of (1, 1, 1) LaAlO_3	17
3.1 Crystal structure	17
3.2 Experiment	19
3.3 Surface morphology of treated substrate	20
Chapter 4. Epitaxial growth of CaTiO_3 film by Pulsed Laser Deposition	25
4.1 Growth conditions	25
4.2 Heteroepitaxial growth of CaTiO_3 on LaAlO_3 without buffer layer	26
4.2.1 Initial growth and surface morphology	26
4.2.2 Structure analysis	30
4.3 Heteroepitaxial growth of CaTiO_3 on LaAlO_3 with buffer layer LaAlO_3	32
4.4 CaTiO_3 film growth with bottom electrode on LaAlO_3	34
4.4.1 Growth studies of SrRuO_3 on LaAlO_3	34
4.4.2 Growth studies of CaRuO_3 on LaAlO_3	36
Chapter 5. Results and discussion	38
5.1 Structure property	38
5.2 Electric properties	43
Chapter 6. Conclusions and recommendations	44
6.1 Conclusions	44

Contents

6.2 Recommendations	45
References	46

Cover: Schematic side view of LaAlO_3 cubic 2 unit cell. The cutting plane is $(\frac{1}{2}, \frac{1}{2}, \frac{1}{2})$, which is consist of Lanthanun and Oxygen. The pink ball is Aluminum, the blue balls are Lanthanum, and the green balls are Oxygen.

Graduation committee:

Chairman
Members

Prof. Dr. ing. D. H.A. Blank
Dr. ing. A.J.H.M. Rijnders
Dr. A.J.A. Winnubst
Ir. J.L. Blok

Chapter 1 Introduction

In this chapter, the basic principle of ferroelectric property will be discussed. Following this, more discussion will take place about a strain induced ferroelectric phase in CaTiO_3 thin film. In the end, the specific objective of this dissertation is outlined, which also includes a brief description of the content.

1.1 Ferroelectricity

Ferroelectricity is a property of certain nonconducting crystals, or dielectrics. It exhibits a spontaneous electric dipole moment, the direction of which can be switched between equivalent states by apply an external electric field. Ferroelectricity has also been called Seignette electricity years ago. Because Seignette or Rochelle Salt was the first material, which was found to show ferroelectric properties in 1920. Since most of its properties are similar to the major properties of ferromagnetic materials, such as magnetization, magnetic domains and magnetic hysteresis, this phenomenon is called 'ferroelectricity', even though the physics behind those two phenomenons is completely different.

Ferroelectric materials are characterized by a reversible spontaneous polarization in the absence of an electric field [1]. Spontaneous polarization in a ferroelectric arises from a noncentrosymmetric arrangement of ions in its unit cell. An electric dipole moment is produced by a shift of the positive ions in the opposite direction of the negative ions. The most common ferroelectrics have the ABO_3 perovskite structure which is shown in Figure1-1. The temperature at which the transition takes place is called the Curie temperature T_C . Above the Curie temperature, these materials have a centrosymmetric structure. Therefore they lose all spontaneous polarization. When the temperature is below the Curie point, a phase transformation takes place from the paraelectric state to the ferroelectric state. The center ion is displaced from its body-centered position and the cubic unit cell deforms to one of the noncentrosymmetric structures, such as tetragonal, rhombohedral, orthorhombic or monoclinic structures. When an alternating electric field is applied to a ferroelectric material, the polarization shows a hysteretic behavior with the applied field (Figure 1-2).

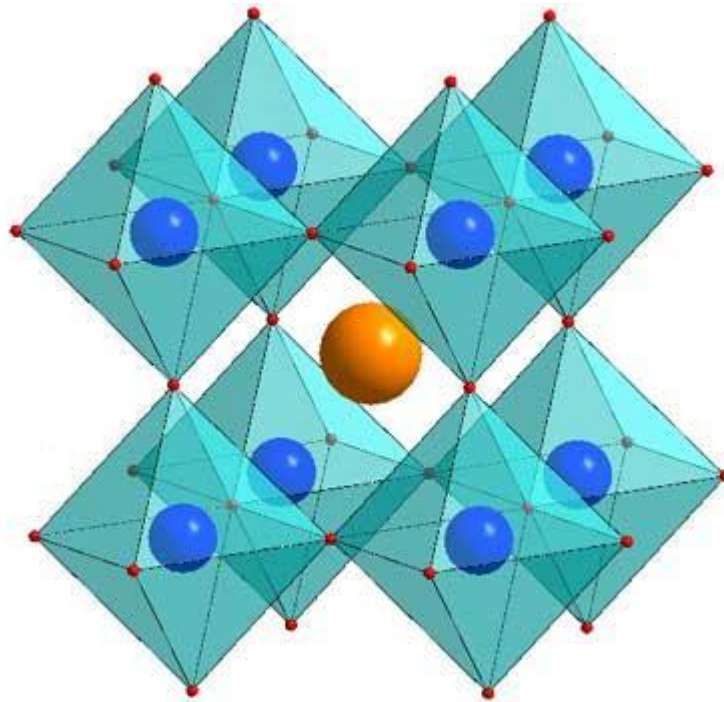


Figure 1-1 Unit cell of ABO_3 type perovskite structured material.

The reversal of polarization can be observed by measuring the ferroelectric hysteresis, which is shown in Fig. 1-2. Assume the starting point to be H. As the electric field strength is increased, the domains start to align in the positive direction giving rise to a rapid increase in the polarization (curve HA). At a very high field level, the polarization will saturate (AB). The state of saturation means all of the dipoles will be aligned parallel and the crystal can be considered as a single domain, in principle. When reducing and reversing the applied electric field the reverse takes place. However, the polarization will not immediately fall to zero when removed the external field. Some of the domains remain aligned in the positive direction when the electric field is zero, and the crystal will show a remnant polarization P_R (OC). The polarization will go to zero when an electric field OE is applied in the negative direction. That external field which is needed to reduce the polarization to zero is called the coercive field strength E_c . If the field is increased to a more negative value, the direction of polarization flips and hence a hysteresis loop is obtained. The value of the spontaneous polarization P_s is obtained by extrapolating the curve (BA) onto the polarization axis.

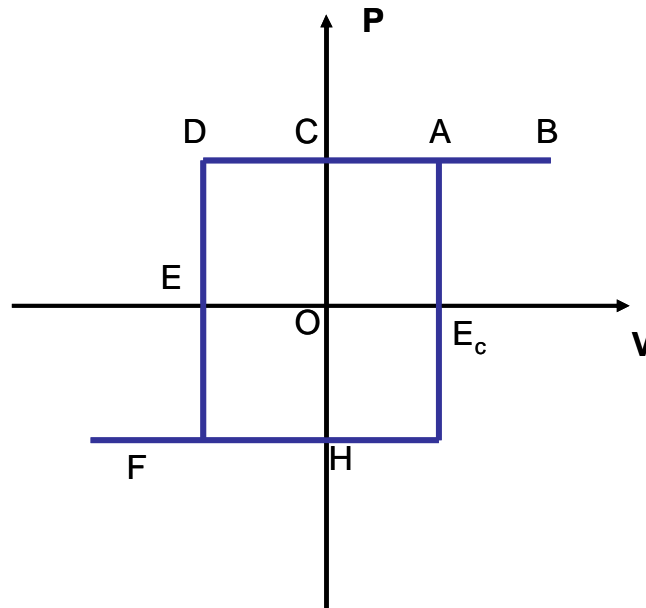


Figure1-2 Ideal hysteresis behavior of the polarization in relation to the applied electric field for typical ferroelectric crystals.

1.2 Ferroelectric phase in CaTiO_3 by epitaxial stain

Perovskite was discovered in the Ural Mountains of Russia by Gustav Rose in 1839 and named for Russian mineralogist, L. A. Perovski (1792-1856). CaTiO_3 belongs to a large ABO_3 perovskite family. In recent years, perovskite oxides are widely used in electronic ceramic materials. Lemanov et al. [2] measured the dielectric properties of CaTiO_3 at temperature from 4.2K to 300K. The dielectric constant increase with decreasing temperature and saturates at low temperatures. CaTiO_3 was classified as an incipient ferroelectric similar to SrTiO_3 , KTaO_3 and TiO_2 .

As reported by Kennedy et al. [3, 4], CaTiO_3 is orthorhombic with space group Pbnm below 1380 K, and belongs to another orthorhombic space group Cmcm between 1380 and 1500 K. At 1500 K, it transforms into tetragonal with space group $14/m\bar{c}m$: Above 1580 K, it becomes cubic with space group $\text{Pm}\bar{3}m$. Wang et al. [5] calculated the density of states, the electric field gradient and the band structure to study the incipient ferroelectricity of CaTiO_3 . From the total calculation, they conclude that CaTiO_3 has a tendency to ferroelectricity in which the Ti atom displaces in the (001) direction. An analysis of the density of states and band structure reveals that there is hybridization between Ti 3d and O 2p. This hybridization is essential leading to the incipient ferroelectricity.

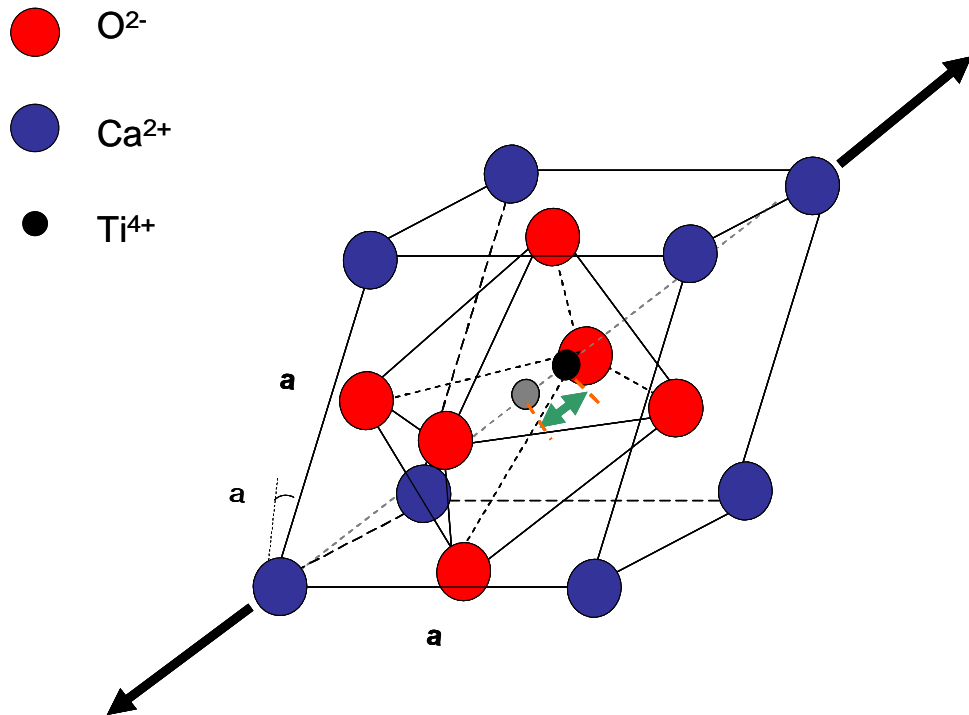


Figure1-3 Switching a cation along (111) direction inside a CaTiO_3 unit cell by applying a voltage. The gray ball in the center is the original position of Ti^{4+} , and the black one is after switching by electric field.

Eklund et al. [6] studied the interaction between two competing structural instabilities in calcium titanate via first principles calculation. The authors compare the distortions of different symmetry modes in ground state CaTiO_3 in their article. A key observation from their research is that the energy function has a minimum corresponding to a structure, while the distortion is along the (111) direction with the trigonal structure and the space group symmetry $R3c$.

A scheme of CaTiO_3 unit cell, which is distorted in the (111) direction, is shown in Figure 1-3. In perovskite crystal structures, polarization results from the displacement of one type of positive ions. From Figure 1-3, the green arrow in the center shows the switch of Ti^{4+} ion along (111) direction of the unit cell. Figure 1-4 shows a schematic of the (111) plane of the $R3c$ structure. The crystal clearly shows a three-fold rotation symmetry along (111) orientation. The lattice parameter of the latter structure is 3.791\AA in cubic configuration.

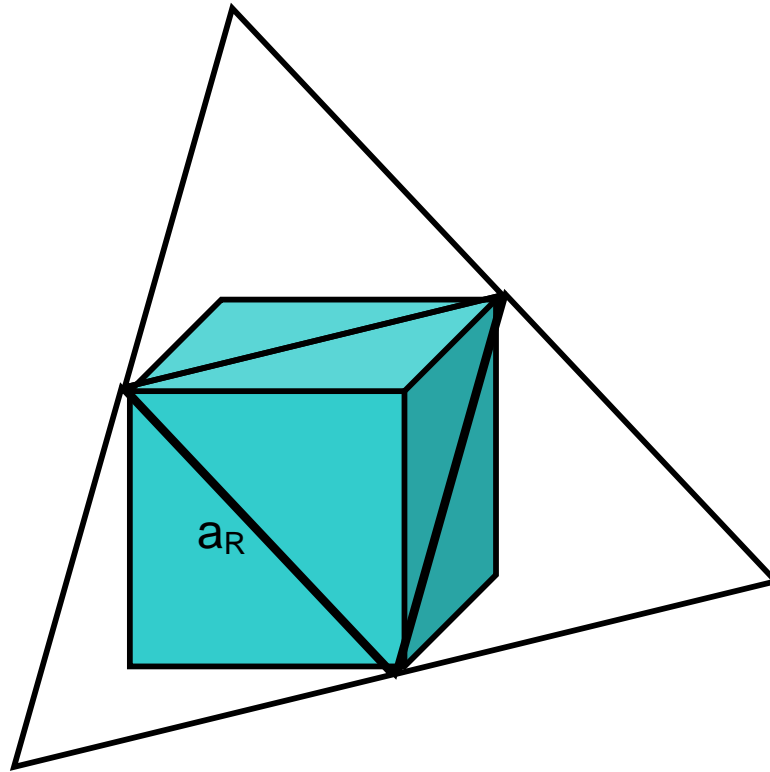


Figure1-4 A schematic depiction of the (111) plane of the $R3c$ structure ($a_R = 5.361\text{\AA}$). The (111) direction has three-fold rotational symmetry.

Eklund et al. [6] showed that this phase has a local energy minimum having a large polarization with both types of instabilities together. The ferroelectric phase of CaTiO_3 may be stabilized by growing a thin film on a hexagonal or trigonal substrate through epitaxial growth, which is the main aim of this thesis.

1.3 Outline

After the initial presentation of general background information in the introduction, this report focuses on relevant theory of CaTiO_3 thin film. It has been reported that oxygen-octahedron rotations tend to suppress ferroelectric instabilities [4]. From the density-functional theory calculation [6], the existence of a metastable ferroelectric phase is close in energy to the orthorhombic ground. It may be possible to stabilize it by growing a calcium titanate thin film on a hexagonal or trigonal substrate. This consideration opens the possibility to artificially stabilize the ferroelectric phase of CaTiO_3 , which is not stable in nature. As far as I know, the epitaxial growth of this kind of film on a hexagonal or trigonal substrate has never been achieved. As a result, it is quite interesting and challenging topic for scientific research.

The main aim of this thesis work is to grow calcium titanate thin films along (111) direction by pulsed laser deposition (see chapter 3). In this project, LaAlO_3 with (111) orientation substrate has been chosen, as the parameter of cubic LaAlO_3 single crystal is close to that of CaTiO_3 single crystal as mention in Figure 1-4. The former is slightly smaller than the latter. In this case, CaTiO_3 will be strained in (111) direction by epitaxial growth on a trigonal substrate.

Since as-received substrates LaAlO_3 have special orientation, different etching procedures have been used to obtain a smooth surface morphology. Next to this, epitaxial growth of CaTiO_3 thin film was realized on (111) pseudocubic LaAlO_3 substrate and structure property and electrical property of CaTiO_3 film were investigated.

The scope and background has been given in Chapter 1, and a list of analysis tools, which is related to this thesis, is mentioned in chapter 2. In Chapter 3, Surface treatment and surface morphology of (111) LaAlO_3 substrate will be discussed. Chapter 4 describes the realization of epitaxial growth of CaTiO_3 film by pulsed laser deposition. Different parameters and different grown models were presented. Chapter 5 provides the characterization of the fabricated artificial structures at different stages of fabrication. Furthermore, a detailed analysis will be presented in this chapter. In chapter 6, a final conclusion will be draw. The recommendations following from this work are presented.

Chapter 2 Fabrication and analysis tools

This chapter presents an overview of the techniques and analysis tools that were used to fabricate and characterize CaTiO₃ thin films. For the fabrication of oxide thin films Pulsed Laser Deposition (PLD) was used. Reflection High-Energy Electron Diffraction (RHEED) was used for in-situ monitoring the growth of thin films. Finally, the analysis tools used in this thesis are: Atomic Force Microscopy (AFM), X-ray Diffraction (XRD) and Transmission Electron Microscopy (TEM).

2.1 Principles of Pulsed Laser Deposition

Pulsed laser deposition (PLD) is a physical vapor deposition technique that uses a highly energetic laser beam to ablate material from target and then transfers to a substrate. When the laser beam hits the target, a dense plasma of material is formed. Due to the high pressure inside the plasma, it expands away from the target and forms a plume. After placing a substrate inside or near the plume, part of the ablation species will form a thin film on the substrate surface. A number of parameters like the absorption coefficient and reflectivity of the target material, the pulse duration, wavelength and energy of the laser beam influence the characteristics of the plume and thus the deposited film. The processes in the plume during transport are influenced by the gas parameters. In order to have a high quality thin film, it is important to control the kinetic energy of the arriving particles and the substrates temperature. In this way, thin film growth can be manipulated.

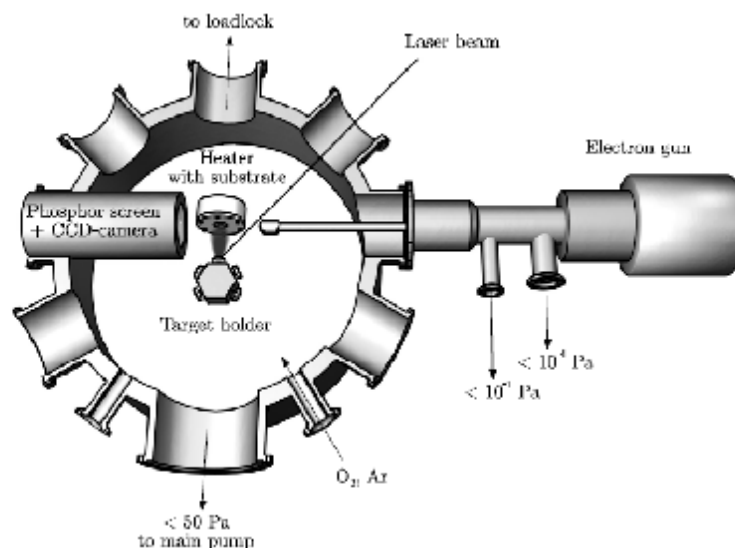


Figure 2-1 schematic drawing of a pulsed laser deposition setup. [14]

A schematic drawing of a PLD chamber is given in Figure 2.1. The laser we used is a pulsed excimer KrF laser with wavelength of 248 nm. The maximum pulse energy is 1000 mJ and width of the laser pulse is about 25ns. The pressure in the vacuum

system during deposition is controlled by the effective pump speed and the total gas mass flow (0 – 40 ml/min). For the deposition gas, both inert gas (Ar) and reactive gases (O_2) can be used. The amount of material ablated from the target surface is determined by the energy density and the spot size. The laser beam is focused onto the target using a lens with a focal length ~ 453 mm. The target holder and heater can be inserted inside the chamber by means of a load-lock system without breaking down the vacuum. Target holder can hold up to 5 targets.

2.2 Reflection High-Energy Electron Diffraction

Reflection high-energy electron diffraction (RHEED) is a very versatile technique for studying the growth and surface morphology of thin films. It provides the information about periodic arrangement of the surface atoms, which is widely used for in-situ measurement of the surface structure during thin film growth. By using a low incidence angle ($1-5^\circ$) for the electron beam, the beam only penetrates a couple of atomic layers. The electrons scattering from a crystal surface leads to a diffraction pattern. A phosphor screen is used to detect the diffracted electrons.

A RHEED pattern from a perfect surface consists of sharp 2D spots, which is lying on the so called Laue circles, see Figure 2-2 (a). In case of a rough surface, the electron beam will penetrate through the islands. The electrons produce a 3D Bragg diffraction pattern, see Figure 2-2 (b).

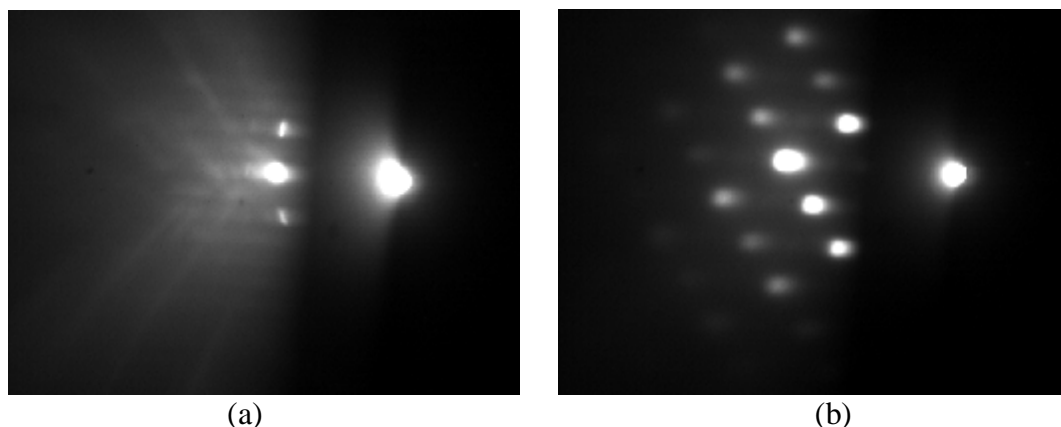


Figure 2-2 RHEED pattern obtain from (a) a treated LAALO₃ substrate (b) a rough surface of CaTiO₃ film.

The intensity of the central RHEED spot (the reflection spot) is used to obtain information about the growth rate. Variation of the RHEED intensity is related to the step density of the sample surface.

2.3 Atomic Force Microscopy

Atomic Force Microscopy (AFM) is a family (together with STM, PFM, MFM etc.) of instruments used for studying surface properties of materials from the atomic to the micron level. During the measurement, the surface of a sample is probed with a

sharp tip, a couple of microns long and often less than 100Å in diameter. The tip is located at the free end of a cantilever. Forces between the tip and the sample surface cause the cantilever to bend or deflect. A detector measures the cantilever deflection as the sample is scanned under the tip. The measured cantilever deflections allow a computer to generate a map of surface topography. AFM can be used to study insulators and semiconductors as well as electrical conductors.

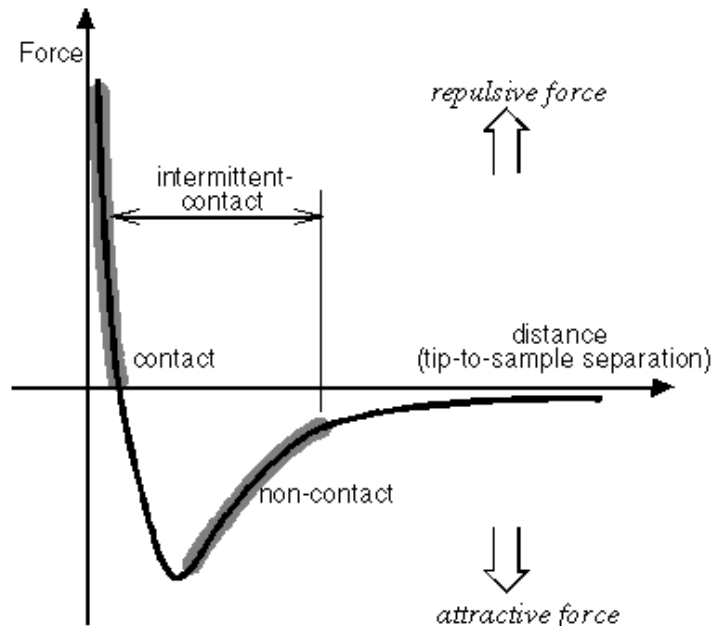


Figure 2-3 Schematic of a generalized Interatomic force vs. distance curve.

Several forces contribute to the deflection of an AFM cantilever. The force most commonly associated with AFM is an interatomic force named the van der Waals force. The dependence of the van der Waals force upon the distance between the tip and the sample is shown in Figure 1. In contact mode AFM measurement, the tip is held less than a few angstroms from the sample surface, and the interatomic force between the cantilever and the sample is repulsive. In non-contact mode AFM measurement, the tip is held on the order of tens to hundreds of angstroms from the sample surface, and the interatomic force between the cantilever and sample is attractive. In tapping mode AFM (TM-AFM) measurement, the tip is brought into intermittent contact region with the sample, which is indicated on the van der Waals curve in Figure 2-3(b). In the following paragraph, the operating principle of the TM-AFM is discussed, since it was used to obtain the surface morphology of the samples presented in this work.

TM-AFM is a vibrating cantilever technique in which an AFM cantilever is vibrated near the surface of a sample. The tip on the vibrating cantilever is brought closer to the sample so that at the bottom of its travel it just barely hits, or "taps," the sample. As for TM-AFM the cantilever's oscillation amplitude changes in response to tip-to-sample spacing. An image representing surface topography is obtained by monitoring these changes. There are two key advantages of TM-AFM. First, it is less likely to damage the sample than contact AFM because it eliminates lateral forces between the tip and the sample. Second, it has been found that TM-AFM is

more effective for imaging larger areas that may have greater variation in sample topography.

2.4 X-ray Diffraction

X-ray diffraction (XRD) is a versatile technique for obtaining detailed information about crystal structure. All the XRD results reported in this thesis were carried out with a Bruker D8 X-ray diffractometer, which is designed to accommodate all X-ray diffraction applications in material research and high resolution diffraction.

Reciprocal space map is a useful scan to distinguish the in-plane and out-of-plane lattices parameters of both film and substrate. The LaAlO_3 substrate used in this thesis was cut in a special orientation (111). In this case, the alignment of reciprocal space was defined as L (111) and H (-101), while H is the in-plane direction and L is the out-of-plane direction. Figure 2-4 shows the area on the reciprocal map that is reachable with the diffractometer. The spot in black is the (321) peak in the reciprocal map. This peak was used for determining the structure in this thesis. The red spots in Figure 2-4 are the reachable points in reciprocal map.

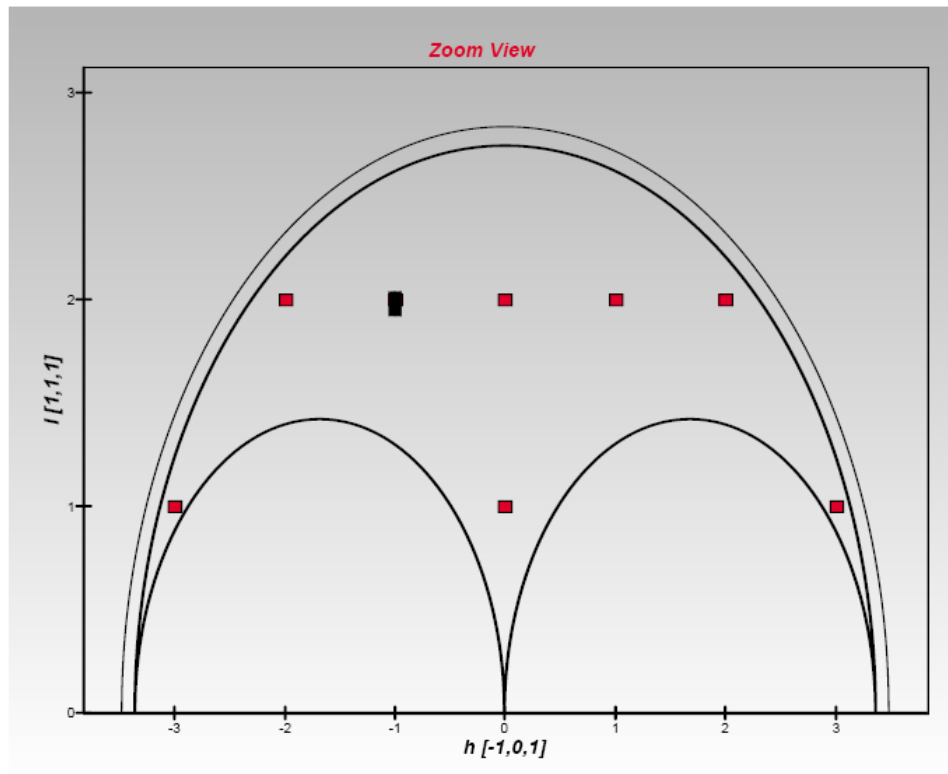


Figure2-4 Reciprocal space map which aligns in L (1,1,1) and H (-1,0,1) in software. The black is the (321) spot in reciprocal map. Reciprocal maps around this spot are studied in this thesis.

2.5 High resolution transmission electron microscopy

High resolution TEM is used to obtain information of the crystal structure and symmetry, which allows the imaging of the crystallographic structure of a sample at an atomic scale. In this thesis, TEM images are used to study the crystal structure and the interface of epitaxial growth.

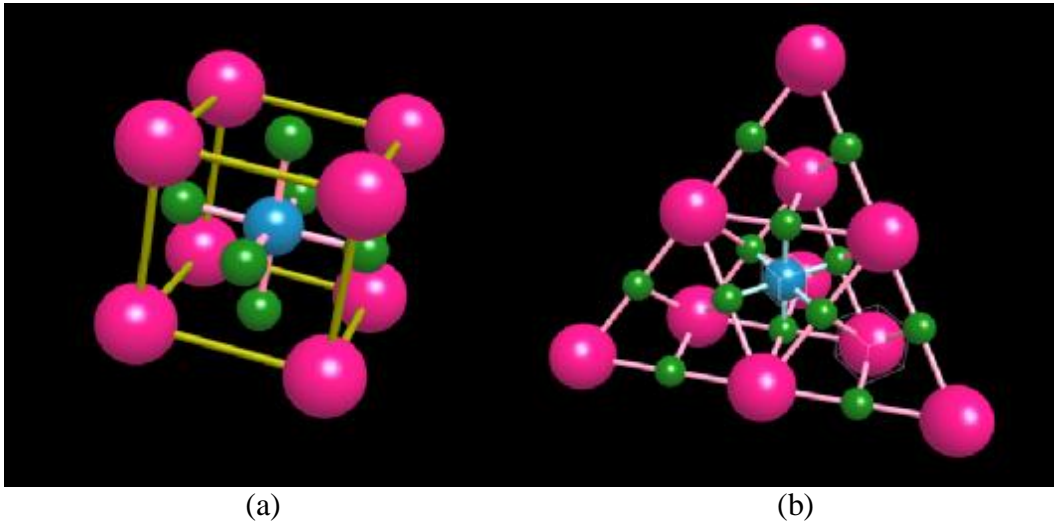
All the images in this thesis were taken on a Philips CM300ST-FEG Twin/STEM, operating at 300 KV. The resolution ($\sim 2.3 \text{ \AA}$) is limited by the image transfer function, which is determined by the instrumental parameters. Cross section images were obtained to study the film and substrates interface region. The specimen in Cross-section was initially thinned by grinding the 3 mm diameter disc down to approximately 50 micron using diamond grinding paper with grit size of 500, 1200 to 2400. The initially thinned sandwich was further prepared using the method of dimple-grinding / dimple-polishing, followed by argon ion etching. Dimple-grinding was accomplished using 1 micron diamond oil paste and a rotating stainless steel grinding wheel. Subsequently, Dimple-polishing was done by applying 1 micron diamond oil paste (approx. 45 minutes.) followed by ultrafine polishing using a 0.02 micron alumina suspension. Argon ion etching was performed in a GATAN model 691 Precision Ion Polisher (PIPS) using subsequently energies of 3.5, 2.5 and ultimately 2.0 kV. Total time spent on preparation is 12 full hours.

Chapter 3 Surface treatment of (1, 1, 1) LaAlO₃

In this chapter, thermal annealing and chemical etching methods are discussed to control the substrates surface morphology. First, the crystalline structure of LaAlO₃ will be described. Then different procedures are discussed to achieve a smooth, single terminated surface. The results will be presented and discussed for each methods under investigation.

3.1 Crystal structure

Lanthanum aluminate (LaAlO₃) single crystals are promising substrates for the epitaxy growth of oxide thin films [8]. Many authors have reported different synthesis methods and potential applications for these crystals [9, 10]. A disadvantage of LaAlO₃ substrates are the formation of twins structures as described by [11]. Kim et al. [12] use TEM investigation to show that (100) twins were formed predominantly over (110) twins. As in many other materials which undergo a phase transition between the rhombohedral one at low temperature and the cubic one at high temperature, the behavior of the phase transition in LaAlO₃ ($T_c=813\text{K}$) has been well studied [13]. Since the transition is of second order, the cubic lattice is distorted along the body diagonal (111) direction and become rhombohedral with no associated volume change[12].



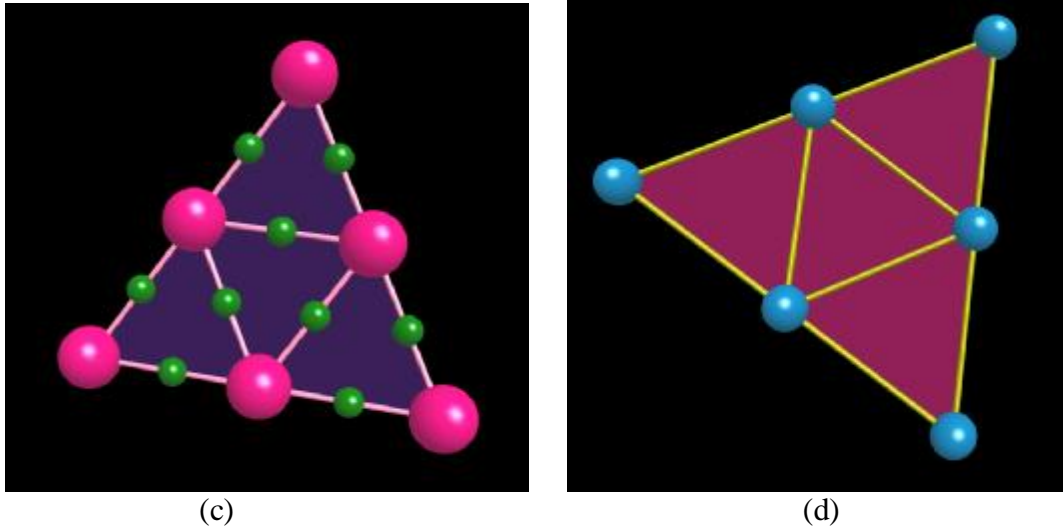


Figure 3-1. Schematic view of LaAlO₃ unit cell. (a) LaAlO₃ cubic unit cell. (b) Top view of LaAlO₃ along (111) direction. (c) Scheme of (LaO₃)³⁺ terminated layer. (d) Al³⁺ terminated layer. (Pink color ball is Lanthanum ions, Blue color ball is Aluminum ions, and Green color ball is oxygen ions).

The unit cell of LaAlO₃ is shown in Figure 3-1 (a). La³⁺ ions (pink color) are at the cube corners, Al³⁺ ion (blue) is in the center of cube and O²⁻ ions (green) are in the face center. In the (111) direction, see Figure 3-1 (b), LaAlO₃ is made up from a stack of (LaO₃)³⁺ layers and Al³⁺ layers. Figure 3-1 (c-d) show the schemes of trigonal like planes, which give the two possible terminations that can be found at the LaAlO₃ substrates surface.

The morphology of as received (111) LaAlO₃ substrates is determined by the polishing method. Different cutting and polishing procedure induces different miscut angle. Figure 3-2 (a) shows the scheme of cutting a LaAlO₃ crystal through the (111) plain, with α is described as the miscut angle. This scheme shows that after normal cutting, a couple of steps will display on top of the surface. The surface of substrates consists of randomly distributed steps with different surface height. In this case, a mix termination of (LaO₃)³⁺ layers and Al³⁺ layers occurs.

To my best knowledge, no articles have been published on treatments for single terminated (111) orientation LaAlO₃ substrates. In order to improve surface morphology, etching and annealing methods have been introduced to control the termination layer. Since aluminum reacts with both strong acid and alkali, while lanthanum oxide only reacts with acid, an alkaline solution is a good choice to remove Al³⁺ layers, see Figure 3-2 (b-c). After the combination of miscut angle, duration for annealing and chemical etching, a single terminated and smooth surface of LaAlO₃ substrates can be obtained.

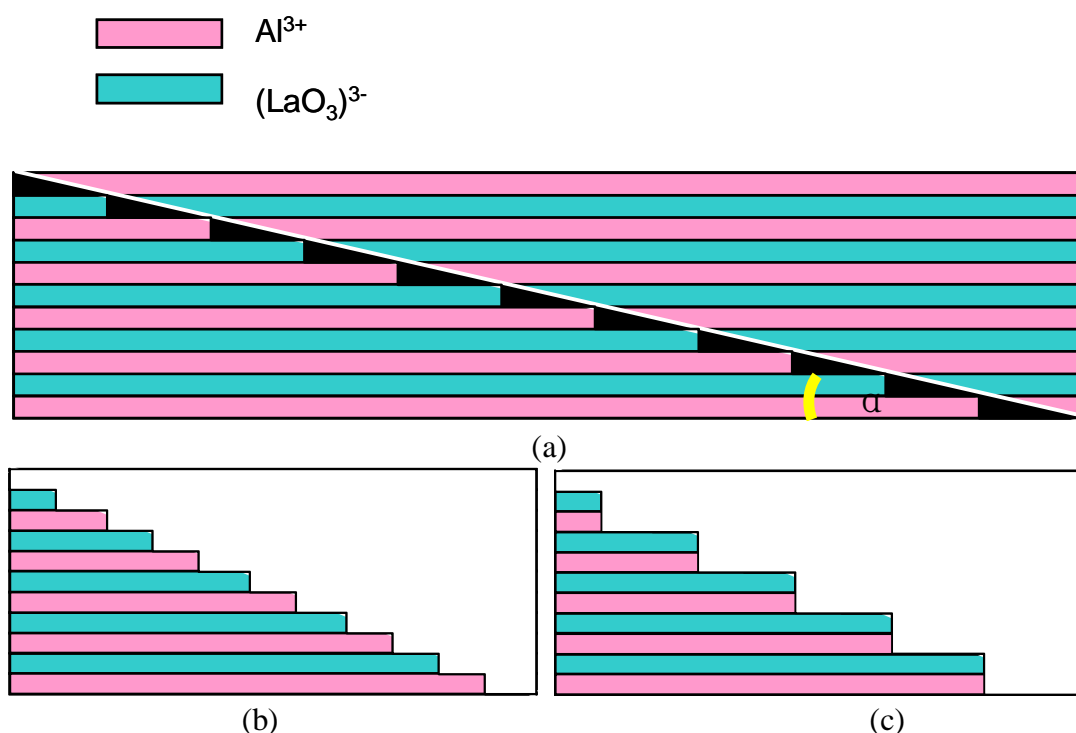


Figure3-2 (a) Schematic drawing of LaAlO₃ substrates, α is the miscut angle. (b) and (c) show the surface termination of LaAlO₃ substrates.

3.2 Experiment

The as-received LaAlO₃ substrates with dimensions of 10×10×1mm³ were cut in pieces of 5×5×1mm³ and 3×3×1 mm³, which were cleaned with chloroform, acetone and ethanol sequentially. After all the cleaning procedures, the substrates were ready for thermal annealing or chemical etching experiments. The annealing experiments of the as-received or chemically etched substrates were performed in a tube-oven with the oxygen flow at a rate of 150 l/h. The annealing temperature was 1000°C.

For chemical etching procedure, an aqueous alkaline solution was taken to etch the Al³⁺ layers. (see Figure3-2 c) The chemical reaction that takes place during etching is:



Due to the high reactivity of the Al³⁺ layer and the solubility in water of the reaction product NaAlO₂, aqueous NaOH solution was chosen as a strong alkali. First the substrates were soaked in aqueous NaOH solution for 15-25 minutes. Then, in ultrasonic bath, these substrates were soaked in a lower concentration NaOH solution, demineralized water and ethanol respectively. The etching experiments were done at room temperature. The concentrations of NaOH solution was changed from 1M to 12M.

3.3 Surface morphology of treated substrate

The surface morphology of an as-received (111) orientation LaAlO₃ substrate is shown in Figure 3-1 (a). Terraces with rough and disordered step ledges are shown in this AFM topographic image. Height analysis indicates the roughness of the surface, while both 0.215nm and 0.11nm step heights are observed, see Figure 3-1 (b). Since the lattice constant of cubic LaAlO₃ is 0.379nm, the distance between (LaO₃)³⁺ layer and Al³⁺ layer in (111) direction is 0.109nm. And the distance between (LaO₃)³⁺ layer and (LaO₃)³⁺ layer or Al³⁺ layer and Al³⁺ layer is 0.219nm. In this case, the as-received substrates have a mixed terminated surface. Figure 3-1 (c) shows an AFM micrograph of an as-received LaAlO₃ substrate that was annealed for 1 hour at 1000°C. After thermal treatment, a clear step-terrace has been observed due to the re-crystallization in high temperature. However, the step ledges are not smooth. The shape of surface defects indicates a mixed termination after thermal treatment. From Figure 3-3 (d), the step edge heights are roughly 0.22nm, which is comparable to the distance from (LaO₃)³⁺ layer to the next (LaO₃)³⁺ layer or from Al³⁺ layer to the next Al³⁺ layer.

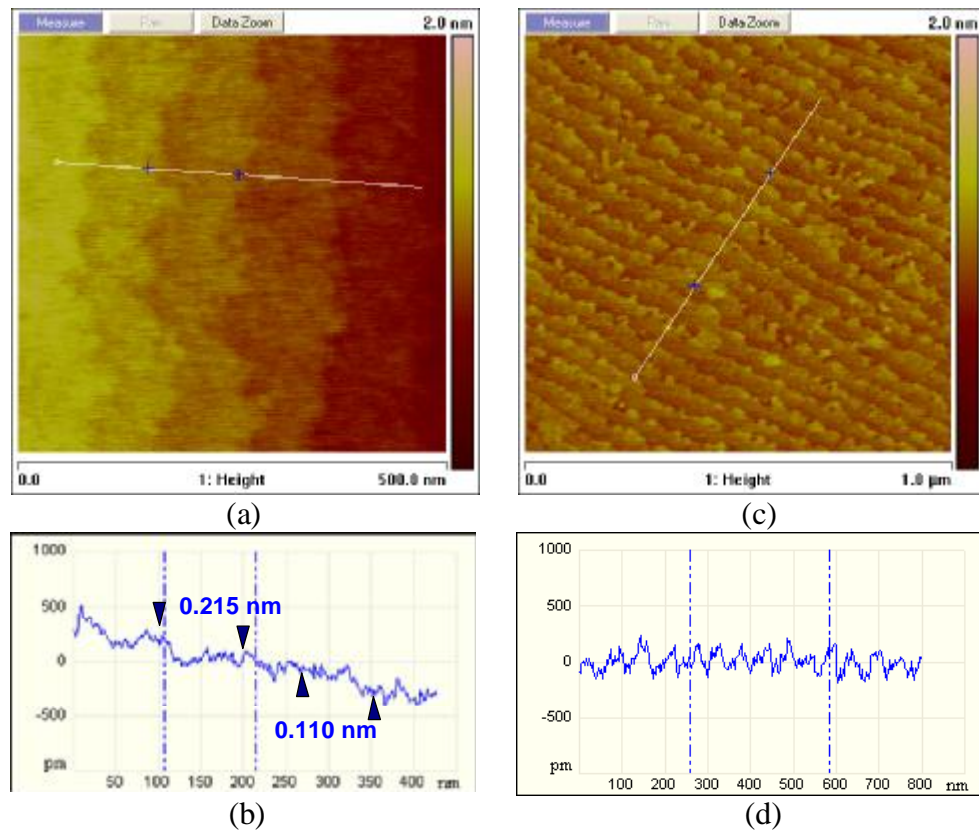


Figure 3-3 AFM micrographs of (111) LaAlO₃ substrates, (a) as-received substrate. (b) Cross-section analysis of (a). (c) Annealed 1 hour at 1000°C in O₂ flow (150 l/h). (d) Cross-section analysis of (c).

Aqueous solution of NaOH was introduced to etching procedure because of the different reactivity of different layers. Figure 3-4 shows the annealed sample before (a) and after (b) etching in 5M NaOH solution. The shape contrast between AFM micrographs and the big holes on the etched surface show that the alkali solution etched the surface layer of (111) LaAlO₃.

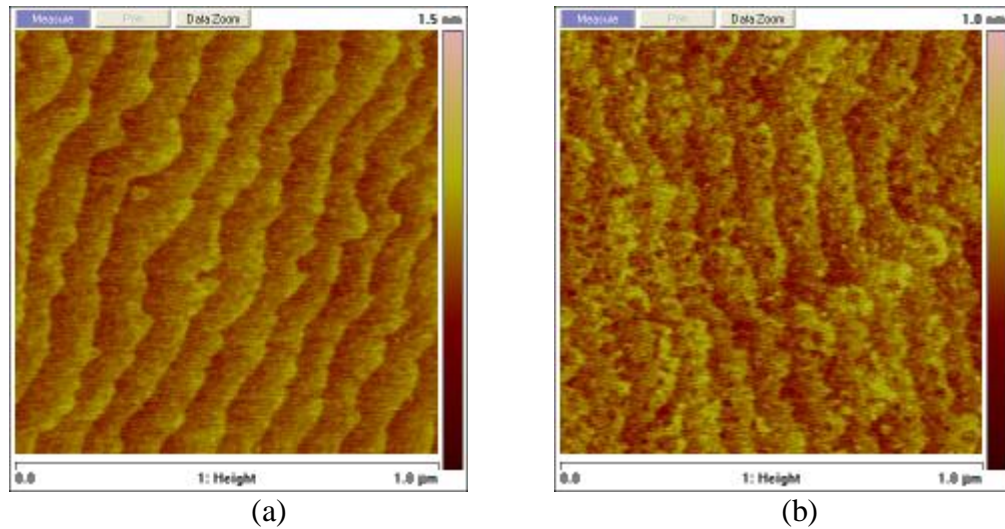


Figure3-4 AFM micrographs of (111) LaAlO₃ (a) annealed at 1000°C for 1 h and then (b) etched 10 min in 5M NaOH. The effect of the etching solution can clearly be seen in (b). According to formula (3.1) The Al layer should have been etched away.

The effect of different surface treatments and alkaline concentrations are shown in Figure 3-5. Figure 3-5 (a) is an AFM micrograph of (111) LaAlO₃ etched with a 1 M aqueous solution of NaOH for 15 minutes. The substrate is then rinsed with demineralized water and ethanol and annealed 1 h at 1000°C under O₂ flow. As mentioned before, the Al³⁺ layer is dissolved in NaOH to achieve a single termination. When substrates were removed from NaOH solution and directly transferred to demineralized water, the significant rise of Ph value (from 14 to 6) convert the AlO₂⁻ to Al(OH)₃ which has poor solubility in water. After annealing at high temperature, Al(OH)₃ turn out to be Al₂O₃, which form a lot of small particles on surface. When increase the concentration of aqueous solution of NaOH, there are more AlO₂⁻ reactant, which caused more particles on substrates, see Figure 3-5 (b). Figure 3-5 (c) shows AFM micrographs of (111) LaAlO₃ etching in 12M aqueous solution of NaOH for 25 min, rinse with low concentration NaOH solution for a couple of minutes, then rinse with demineralized water. After annealed in oven at 1000°C for an hour, a clear and regular step terrace without any particles is obtained.

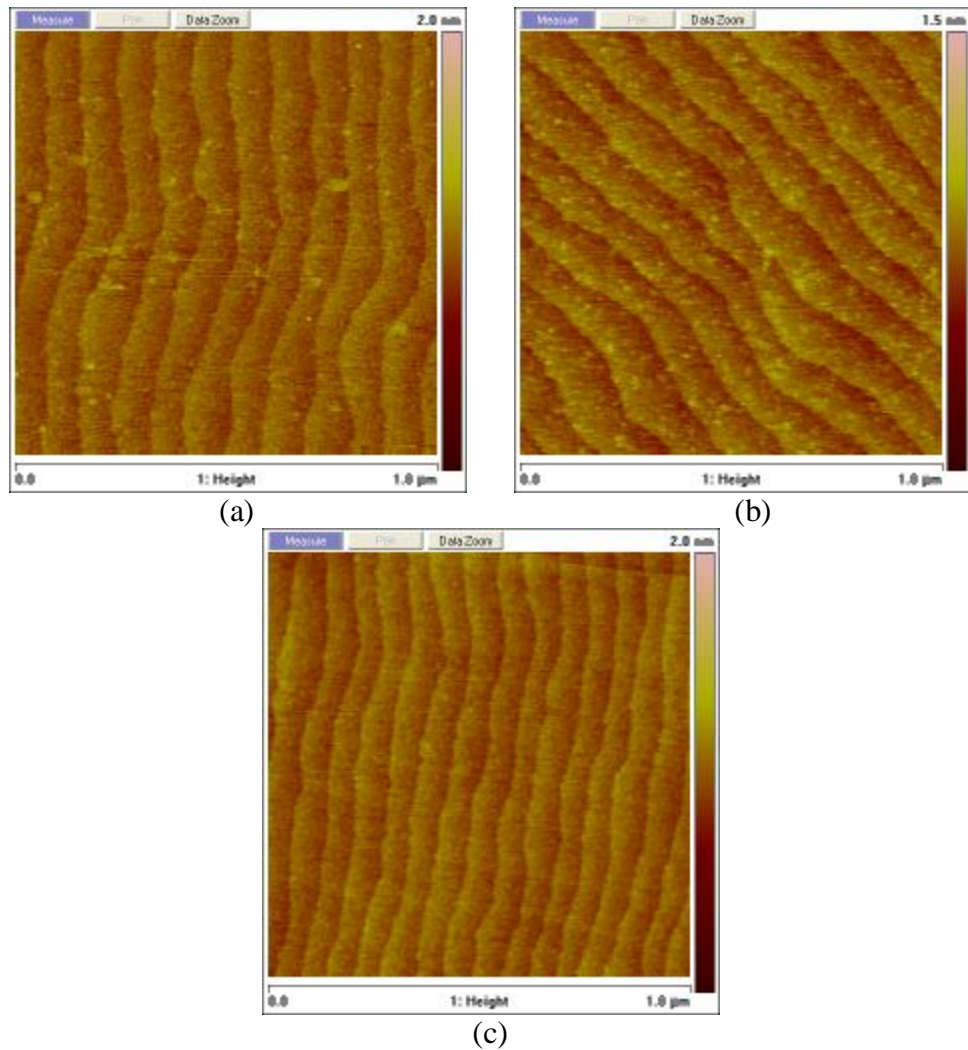


Figure 3-5 AFM micrographs of (111) LaAlO_3 etching in aqueous solution of NaOH. Etching conditions (a) 15min in 1M NaOH. (b) 15min in 10M NaOH. (c) 25min in 12M NaOH then 15min in 4M NaOH.

Besides different concentration etchant and different etching time, other conditions, such as annealing time and miscut angle all influence the actual shape of the step edges and roughness of surface. Figure 3-6 a-d show the AFM micrographs of (111) LaAlO_3 substrates with different anneal time after the constant etching concentration. A curved shape of step ledge and a lot of surface defects are obtained with short anneal time, see Figure 3-6 a-b. In Figure 3-6 c-d, step bunching and incomplete removal of surface layer are observed with long anneal time. The miscut angle of the substrates we used in this thesis is around 0.15-0.25. In this miscut angle range, one hour was found to be the optimal anneal time for the etched substrates, compare to Figure 3-7. If the miscut angle is smaller, the anneal time should be longer and vice versa.

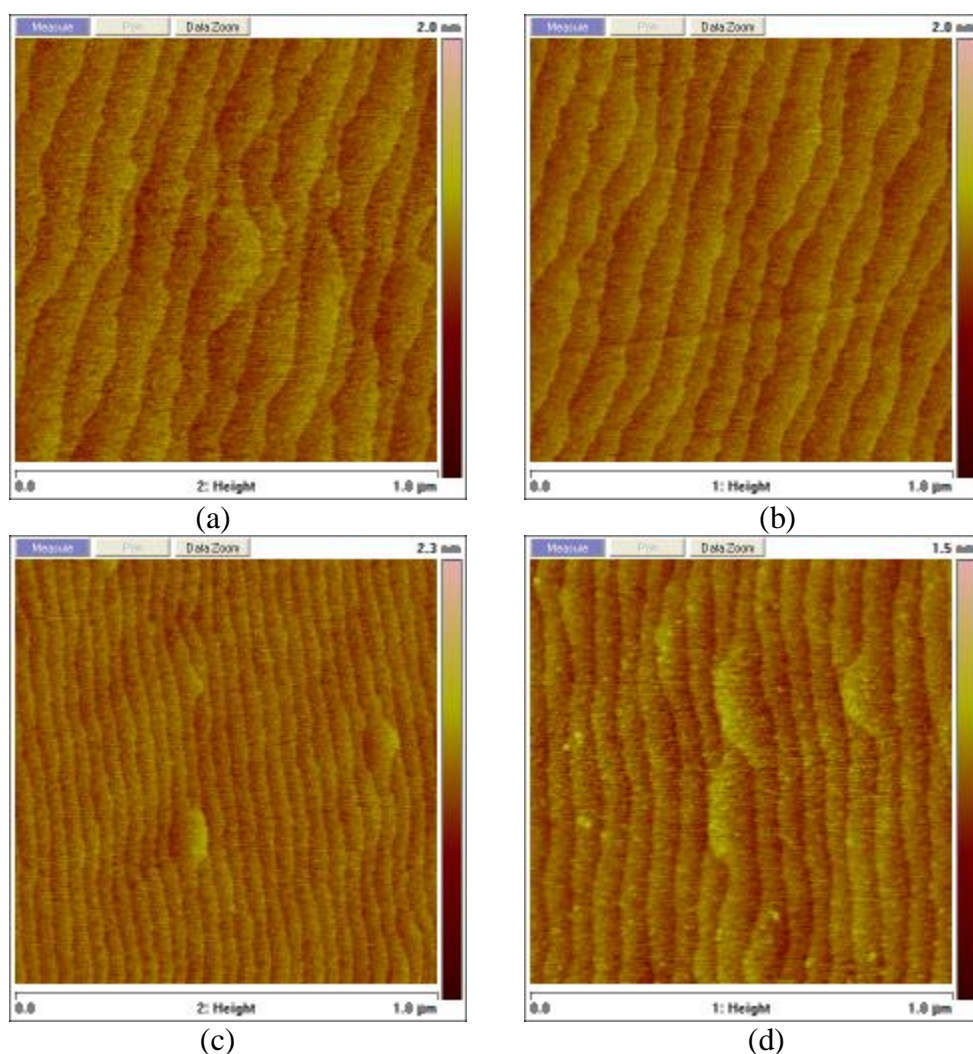
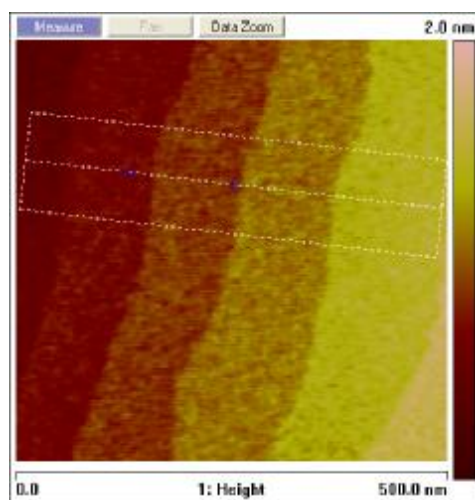
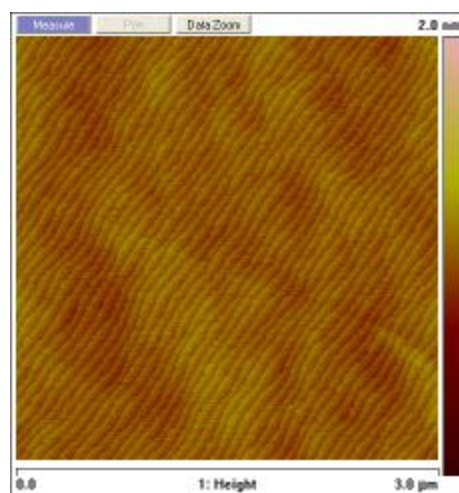


Figure 3-6 AFM micrographs of (111) LaAlO₃ substrates Etched 25min in 12M NaOH and 15min in 4M NaOH, then annealed at 1000°C in O₂ flow for (a) 30 minutes (b) 50 minutes (c) 70 minutes and (d) 120 minutes.

Figure 3-7 shows the AFM surface morphology in the optimal condition. A flat surface and a smooth step terraced were observed. Height profile show the height steps on the terraces are 0.218 nm, which is equal to the distance between (LaO₃)³⁺ layer and (LaO₃)³⁺ layer. The friction of AFM images of this treated substrates did not show any contrast, which indicate that smooth and single terminated substrates were obtain after chemical and thermal treatment.



(a)



(b)



(c)

Figure3-7 AFM micrographs of (111) LaAlO_3 substrates etched 25min in 12M NaOH and 15min in 4M NaOH, then annealed 1 h at 1000°C in O_2 flow. Height profile shows the height islands on the height terraces is 0.218 nm.

Chapter 4 Epitaxial growth of CaTiO₃ film by Pulsed Laser Deposition.

In this chapter, different growth conditions and growth modes are discussed for epitaxial growth of CaTiO₃ thin films. A buffer layer of LaAlO₃ is introduced to improve the substrate surface morphology. Oxide bottom and top electrodes were grown for the purpose of electrical measurements that are discussed in the next chapter.

4.1 Growth conditions

CaTiO₃ thin films were grown epitaxially on (111) LaAlO₃ substrates by the pulsed laser deposition technique. The PLD system, together with in situ RHEED was used in these experiments (more details see Chapter 2). The growth conditions of CaTiO₃ were chosen according to the growth of titanite oxide, reported previously [15]. A laser with wavelength 248nm was used, while an optimum laser fluency of 1.3 J/cm² and a pulse repetition rate of 1 Hz were selected. The target and substrate distance was fixed as 50mm. The background pressure was 0.03 mbar O₂. The substrates used in deposition were cleaned in organic solvents and treated by using the procedures described in Chapter 3. The substrates were attached to the heater by silver glue. The growth and thin film thickness were monitored in situ by monitoring the RHEED intensity oscillations of the specular reflected spot.

Using the above deposition conditions and a substrate temperature range from 700°C to 850° and a different size of the mask (different areas of mask cause different spot size on target), which is placed in the laser beam, are used to optimize the LaAlO₃ growth. Typically, the RHEED intensity shows the first few monolayers as initial 2 D growth. This is followed by a sharp drop in intensity and 3 D patterns, which indicate the film surface become roughened. The maximum numbers of oscillations achievable during the different deposition conditions are shown in Figure 4-1. As can be seen from this graph different temperatures and different spot sizes have a large influence on the film growth. At a temperature above 750°C, a decreasing number of oscillations are obtained with increasing temperature. Figure 4-1 shows that 750 °C is the best temperature for the growth of CaTiO₃. The spot size also plays an important role for film growth, since a bigger spot size bring much more materials to the substrate for each pulse compared to a small spot size, while the small spot size gives less flux. However, Figure 4-1 shows that a bigger spot size does not increase the number of oscillations. Therefore, a mask area of 30mm² with a spot size 1.102 mm² is the optimum parameter for CaTiO₃ film.

During cool down, the LaAlO₃ films were annealed in 1 bar oxygen pressure while ramping down the temperature with 10 deg/min. A high oxygen pressure is necessary to remove oxygen vacancies in the film.

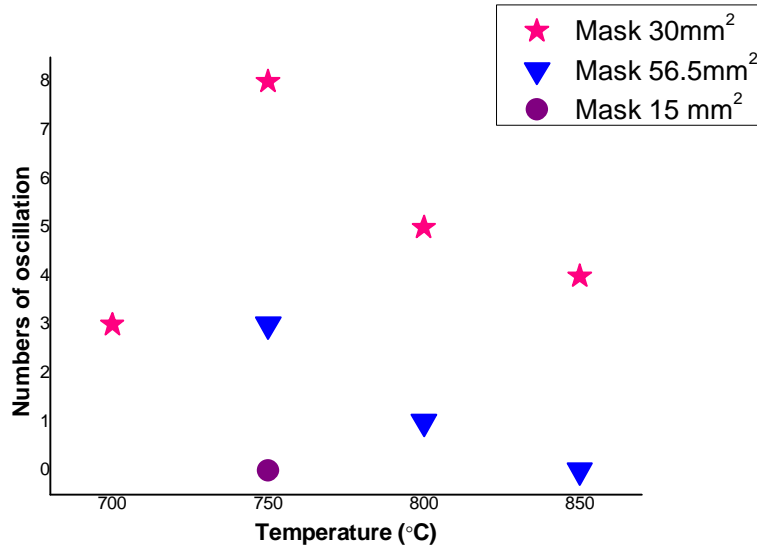


Figure4-1 the maximum numbers of oscillation of RHEED intensity changes with different temperatures and different spot sizes.

The deposition of LaAlO_3 buffer layer was introduced in section 4.3. The condition for LaAlO_3 deposition on (111) LaAlO_3 substrates was the same as CaTiO_3 film growth. The only different between these two depositions are the heater temperature, which is 850 °C for LaAlO_3 buffer layer [16].

Further more, two kinds of electrode materials (SrRuO_3 , CaRuO_3) were used to grow as bottom and top electrodes for measuring the electric properties of CaTiO_3 thin films. The same deposition conditions were used to grow SrRuO_3 and CaRuO_3 film. The background O_2 pressure is 0.13 mbar for bottom electrode and 0.075 mbar for top electrodes, with a temperature is 700 °C for bottom electrode and 500 °C for top electrode [17]. An optimum fluency is 2.5 J/cm^2 , with a frequency of 2 Hz. The bottom electrode growth can be monitored by RHEED system.

Using the PLD condition discussed above, an epitaxial CaTiO_3 film can be grown on (111) treated LaAlO_3 substrates (miscut angle 0.15~1.25, which is measured by X-ray diffraction). The surface morphology was analyzed by atomic force microscopy. X-ray diffraction (Chapter 5) and high-resolution TEM were used for structural characterization of CaTiO_3 thin film (Chapter 4).

4.2 Heteroepitaxial growth of CaTiO_3 on LaAlO_3 without buffer layer

4.2.1 Initial growth and surface morphology

Figure 4-2 shows the RHEED intensity during CaTiO_3 growth on (111) LaAlO_3 substrates of four unit cell lays. The initial CaTiO_3 deposition indicates a 2-

dimensional growth. The oscillation period in RHEED intensity is 25 pulses. The deposition was stopped just in the maximum of the fourth oscillation. The insets in Figure 4-2 shows RHEED pattern before and after deposition. The first one is the RHEED pattern of a treated LaAlO_3 substrate, which provides the information of a crystalline and smooth substrate surface. The splitting of one side of RHEED spots is probably due to the twins' structure of LaAlO_3 . The RHEED pattern after deposition still shows clearly two-dimensional spots. These RHEED patterns indicate that 4 unit cell CaTiO_3 thin film surface is smooth and crystalline.

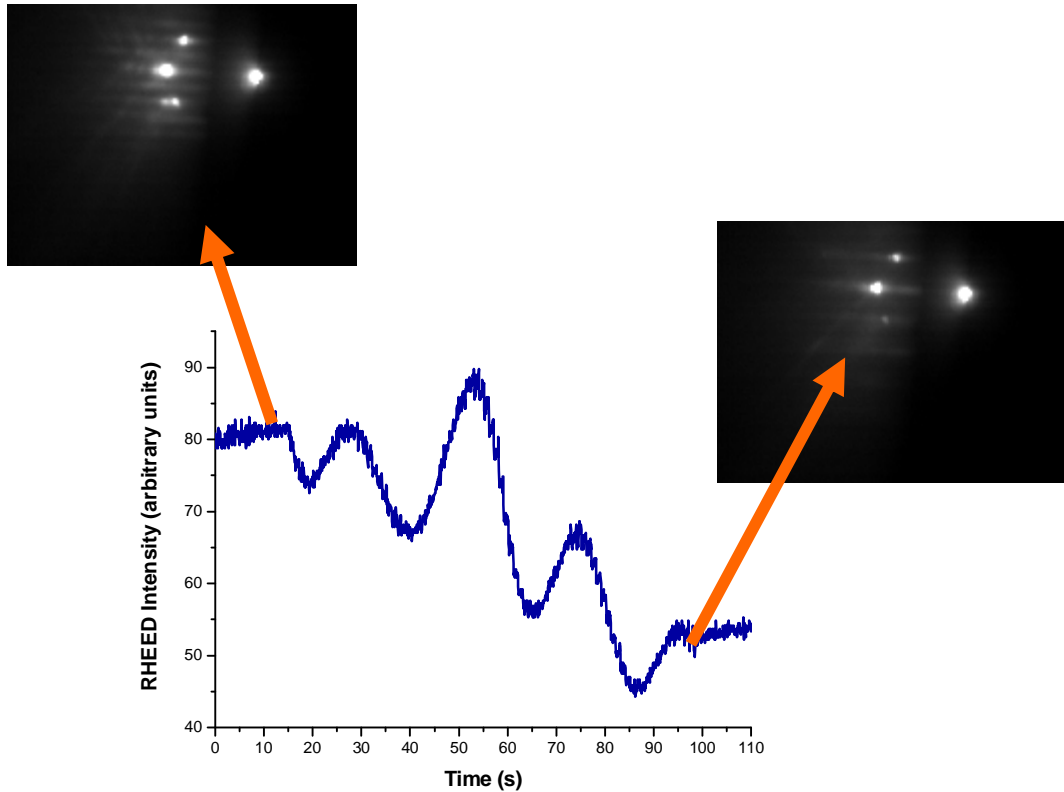


Figure 4-2 RHEED intensity of the central RHEED spot during growth CaTiO_3 on (111) LaAlO_3 substrate. The insets show the RHEED pattern obtained before and after deposition.

The AFM micrograph of the CaTiO_3 thin film is displayed in Figure 4-3, which shows a smooth terrace structure. The height between each step is 0.219 nm, see the cross section analysis from Figure 4-3, which is equal to the distance of one unit cell CaTiO_3 along (111) direction. The flat surface image indicates that the first 4 unit cells have in 2D growth mode on a treated LaAlO_3 substrate, which in agreement with the observation of the RHEED intensity, see Figure 4-2.

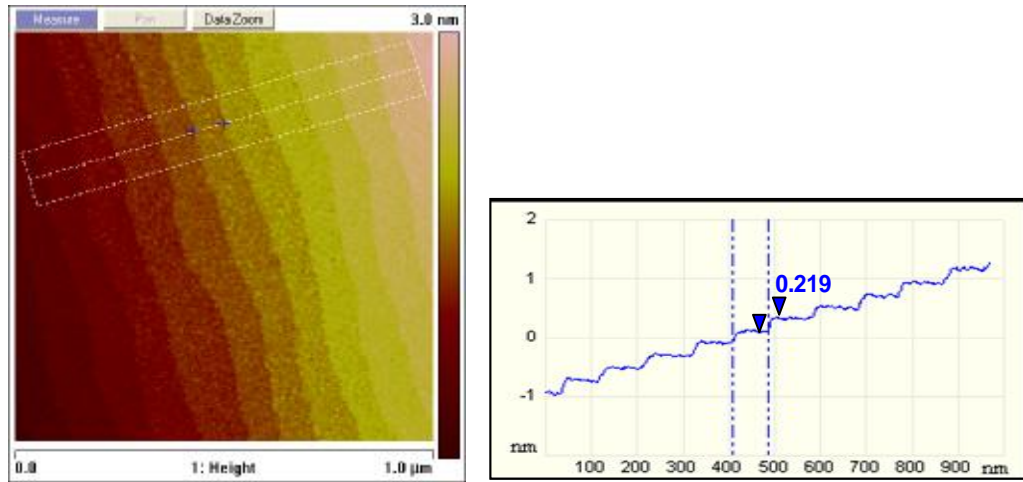


Figure 4-3 Surface analysis by atomic force microscope of a 4 unit cell thick CaTiO_3 thin film on LaAlO_3 substrates. The section analysis of the selected box shows smooth terraces with steps.

A CaTiO_3 thin film of 50 nanometer thickness was epitaxial grown on (111) LaAlO_3 substrates. The RHEED intensity as a function of time during growth is plotted in Figure 4-4. The optimum conditions discussed in the previous section were used. The oscillation intensity is found to be dropping rapidly after the seventh oscillation. The RHEED pattern shows a 3D pattern after 5 minutes deposition, which agrees with the rough surface found in the AFM measurement in Figure 4-5. However, unlike the normal intensity curve, Figure 4-4 shows that the oscillation of the first monolayer is slightly lower than that of the second monolayer one, this is seen consistently for all films. It indicates the growth of the first monolayer is different from the second, which is opposite to the normal situation of heteroepitaxial growth. To explain the growth at the interface, TEM image in Figure 4-6 was used.

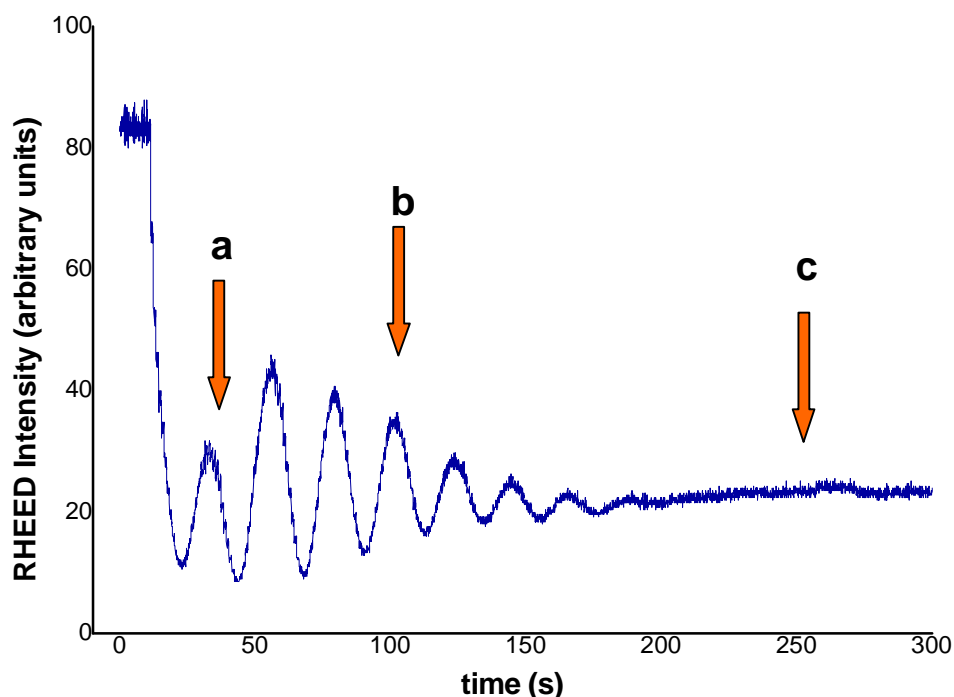


Figure 4-4 RHEED intensity of the central spot is taken during growth CaTiO_3 thin film at 750°C , which shows eight oscillations at the beginning.

Figure 4-5 shows the ex-situ AFM morphology of CaTiO_3 films with thicknesses of 1 unit cell, 4 unit cells, 10 unit cells and 50nm, while (a), (b) and (c) are relative to the arrowhead position in Figure 4-4, d is taken at the end of the deposition. In Figure 4-5 (a) and (b), the step and terrace structure of the substrates were preserved during depositions, which is consistent with the oscillation from RHEED pattern. The surface in Figure 4-5 (c) is much rougher than the surface in image of (a) and (b), this agrees with the damping of the oscillations after approximately 8 unit cell. Figure 4-5 (d) shows the AFM image after grown 50nm CaTiO_3 film on (111) LaAlO_3 . The high roughness on the surface confirms the 3-dimensional RHEED pattern, which was obtained after 50nm film. To summarize, layer by layer growth is achieved in the first several monolayers, which indicates that the film is strained onto the LaAlO_3 substrate (for more details, see structure analysis). After the first 8 monolayers the growth mode changes to island growth. At this point it is not known from the RHEED signal whether the film relaxes or not.

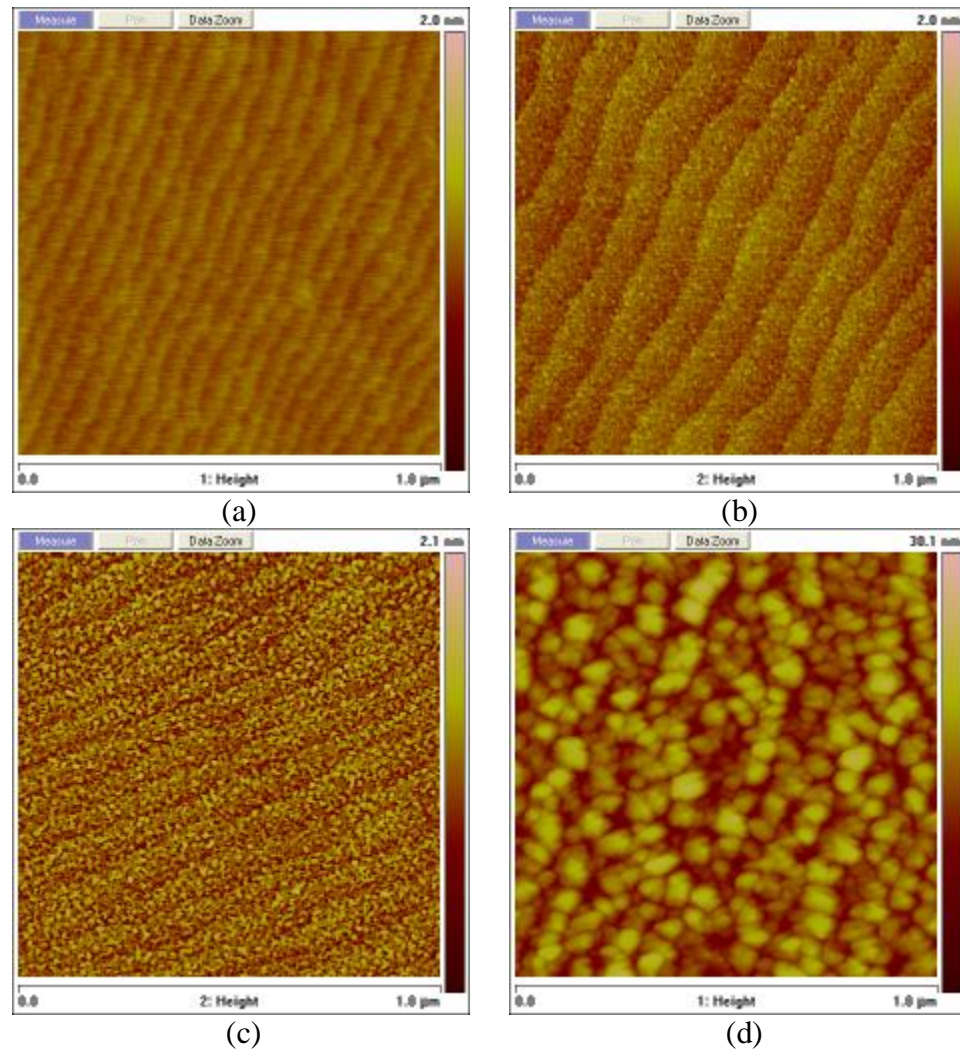


Figure 4-5 AFM micrographs after deposition CaTiO_3 on LaAlO_3 substrates at 750°C of (a) 1 unit cell layer (b) 4 unit cell layers and (c) 10 unit cell layers. (d) After deposition of 50 nm CaTiO_3 film. (a) (b) and (c) are relative to the arrowhead in Figure 4-4.

4.2.2 Structural analysis

To comprehend the RHEED intensity and AFM morphology of the strange first monolayer on (111) LaAlO_3 , high-resolution TEM was used to analyze the interface structure. Cross section High resolution TEM was taken along the interface of CaTiO_3 thin film and LaAlO_3 substrates see Figure 4-6. The dark part on top is LaAlO_3 substrate, while the light part is CaTiO_3 film. The distance between the white lines drawn in Figure 4-6 is equal to 20 unit cell, which shows the same numbers of unit cell in substrate as that in the film. It shows epitaxial growth of the CaTiO_3 thin film directly on (111) LaAlO_3 .

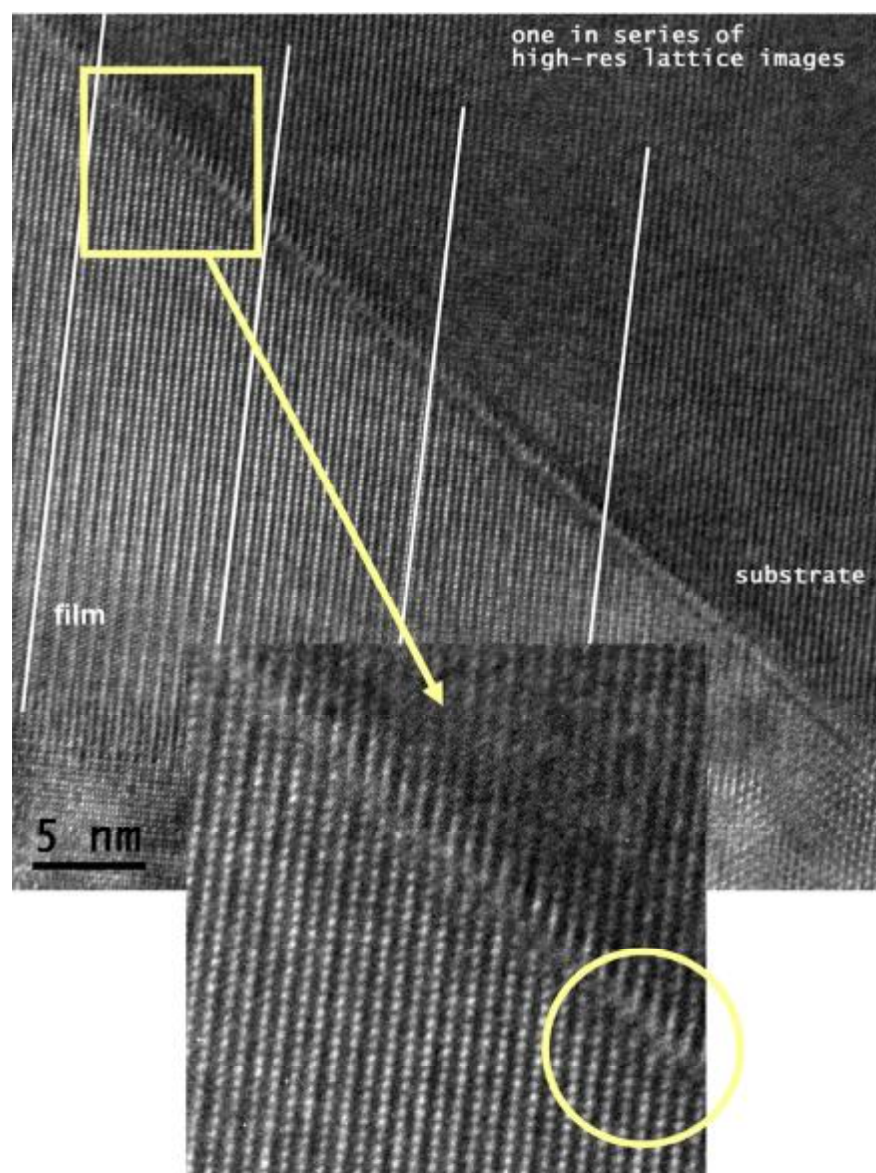


Figure 4-6 Cross-section High resolution transmission electron microscopy analysis of CaTiO_3 film on LaAlO_3 substrate. Straight lines drawn show the similar unit cell size between film and substrate. The bottom image is the magnified image of the yellow square of the top image. The yellow circle in the bottom image indicates the dislocation of film growth in the first unit cell.

However, from the detailed information in the zoomed image below, the appearance of dislocations at the interface is observed, see the yellow circle. Some parts of the interface show coherent growth, while the other parts of the interface show dislocated lattice growth. This dislocation is probably because of the high charged surface of (111) LaAlO_3 and the misfit between CaTiO_3 and LaAlO_3 . The irregular interface shown in the TEM image gives an explanation for the RHEED oscillation in Figure 4-4, which indicates the growth of the first monolayer is different from the second monolayer.

From the analysis above, it can be seen that, at the initial growth stage, the deposition of the first monolayer does not show a completely coherent growth. In

order to improve it, a LaAlO_3 buffer layer was introduced in the CaTiO_3 heteroepitaxial growth.

4.3 Heteroepitaxial growth of CaTiO_3 on LaAlO_3 with buffer layer LaAlO_3

From the results in last section, the interface between the LaAlO_3 and CaTiO_3 in the TEM picture shows clearly dislocations. We tried to improve the substrate surface by first growing a LaAlO_3 buffer layer on the substrate. The RHEED data of CaTiO_3 thin film grow on LaAlO_3 substrate with a buffer layer of LaAlO_3 is shown in Figure 4-7 (a). The deposition was stopped at the maximum of the third oscillation, which means that three monolayers of LaAlO_3 have been grown. The period of the each oscillation is 25 pulses. The inset RHEED pattern is recorded after deposition. The clear two-dimensional spots indicate a crystalline and smooth surface. As expected, the deposition of LaAlO_3 on LaAlO_3 substrate follows a layer by layer growth mode.

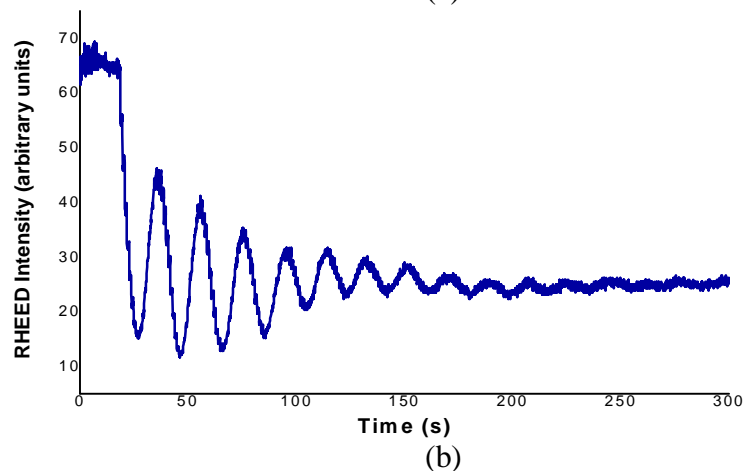
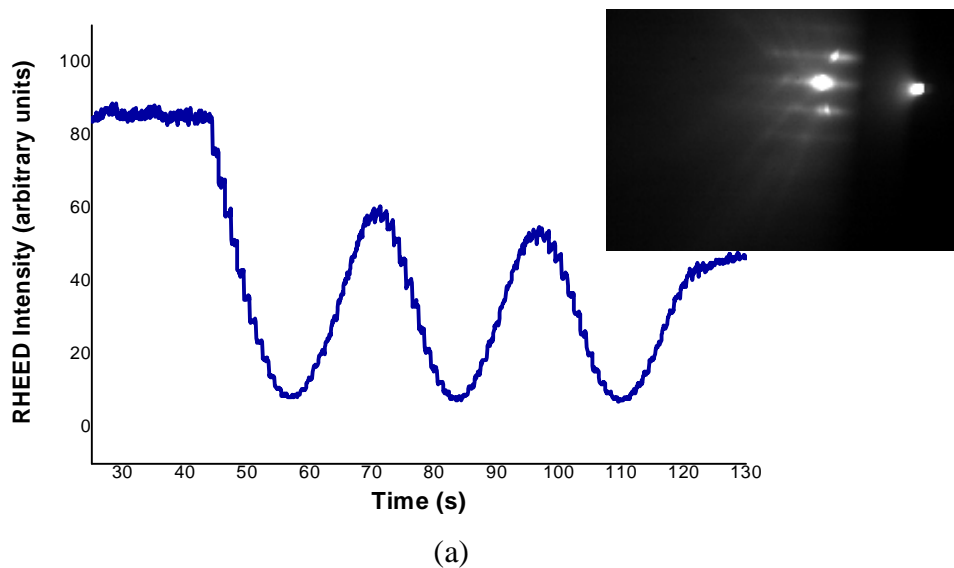


Figure 4-7 RHEED intensity of the central spot during (a) growth 3 monolayers LaAlO_3 at 850 °C. (b) Growth CaTiO_3 thin film after LaAlO_3 buffer layer at 750 °C. The inset shows the RHEED pattern obtained after deposition.

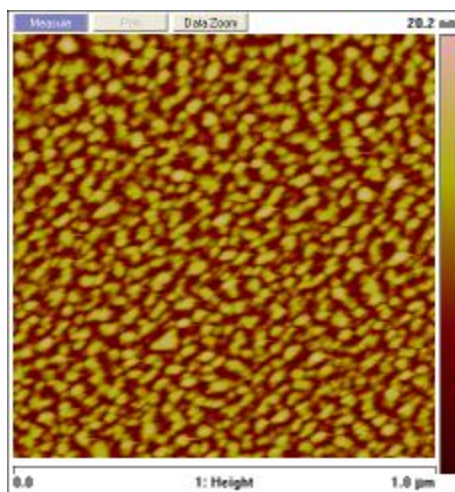


Figure 4-8 AFM micrographs after deposition CaTiO_3 on LaAlO_3 substrates at 750°C with LaAlO_3 buffer layer.

The RHEED intensity recorded during CaTiO_3 growth is shown in Figure 4-7 (b). The growth condition is similar to the previous one without buffer layers and the period of the RHEED oscillations was consistent. More oscillations were achieved in this type of deposition compared to the one in Figure 4-4. It further more illustrates that the intensity of the first oscillation is higher than the second one, and intensity oscillations are damped after deposition of approximately 14 unit cell layers, which indicate the roughness of surface is increase with the decrease of intensity during growth.

The surface morphology of 20nm CaTiO_3 thin film on LaAlO_3 substrate buffered with 3 monolayers of LaAlO_3 is shown in Figure 4-8. The roughened surface with a lot of islands is observed with an average height of 10nm, see the color scale in the right side of the image. According to the AFM micrograph, after the initial growth stage the CaTiO_3 films deposited on the buffered LaAlO_3 substrates do not show an improvement of the surface morphology of CaTiO_3 film.

The Cross section high resolution TEM image of this film is shown in Figure 4-9, which shows the effect of LaAlO_3 buffer layer. There is no dislocation in the interface as compare to Figure 4-6. The area between two arrowheads is the buffer layer interface. The atomic stacking shows a coherent growth, see from the yellow rectangle in Figure 4-9. The CaTiO_3 film is full strain on LaAlO_3 substrate with LaAlO_3 buffer layer. The expected difference of CaTiO_3 growth with and without buffer layer is displayed clearly in Figure 4-9 compare to Figure 4-6. The result shows that the initial CaTiO_3 film growth on the LaAlO_3 buffer layer leads to a good quality of coherent growth, since the LaAlO_3 buffer layer improves the surface morphology of substrate.

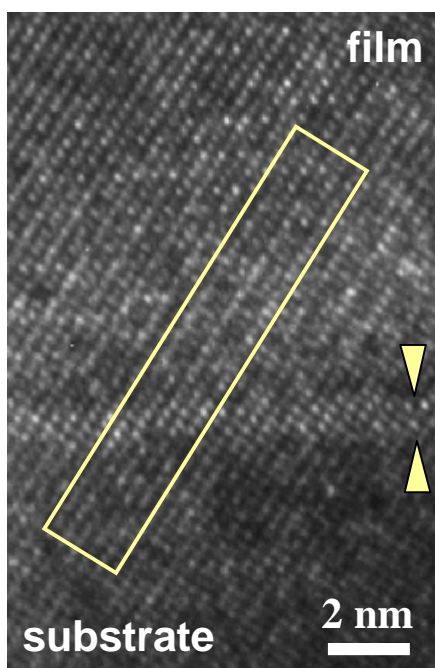


Figure 4-9 Cross-section High resolution transmission electron microscopy analysis of CaTiO_3 film on LaAlO_3 substrate with buffered LaAlO_3 layer. The area in two arrowheads is the LaAlO_3 buffer layer.

4.4 CaTiO_3 film growth with bottom electrode on LaAlO_3

4.4.1 Growth studies of SrRuO_3 on LaAlO_3

In order to measure electric properties, electrodes are necessary to be grown on both sides of the film. The growth of SrRuO_3 bottom electrode on (111) LaAlO_3 substrates is studied in this section. After deposition of the LaAlO_3 buffer layer LaAlO_3 , SrRuO_3 was grown by PLD with the parameter shown in 4.1. The RHEED patterns recorded during and after deposition are depicted in Figure 4-10. At the beginning of deposition, the RHEED intensity increases constantly until it reach a certain level, while the RHEED pattern shows a 3D pattern in Figure 4-10 (a). Subsequently, a blurred streaky pattern is observed after deposition for 13 nm thickness, see Figure 4-10 (b). The streaky RHEED patterns last till the end of SrRuO_3 growth, see Figure 4-10 (c), which indicate a SrRuO_3 film surface with a high step density. From the RHEED signal, a step flow mode is observed till the end of deposition of the SrRuO_3 .

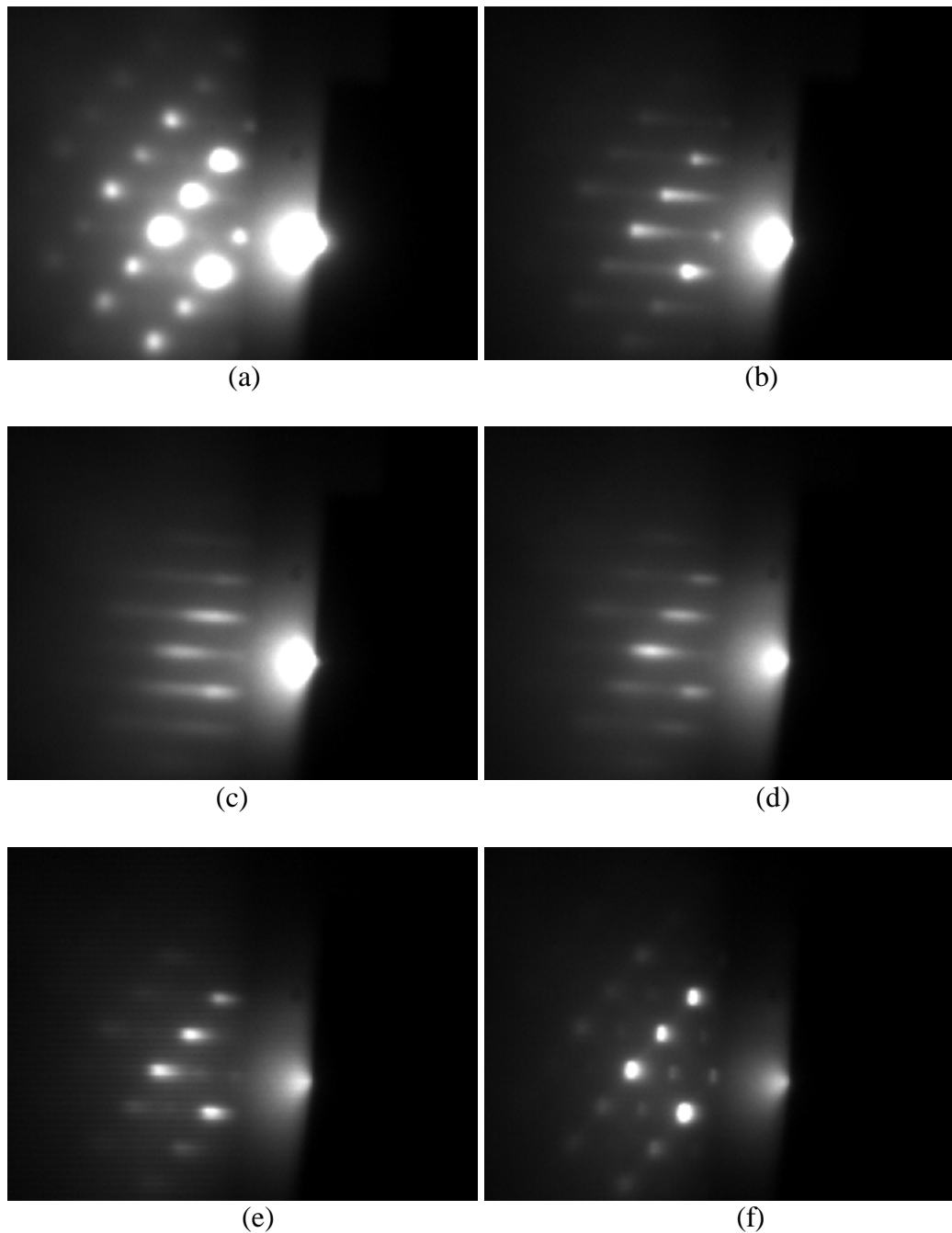


Fig 4-10 RHEED pattern during deposition SrRuO_3 electrode for different thickness (a) 3 nm (b) 13nm and (c) 40 nm. RHEED pattern during deposition CaTiO_3 on top of electrode for different CaTiO_3 thickness (d) 0.7nm (e) 2 nm and (f) 45nm.

After growing a SrRuO_3 bottom electrode, a CaTiO_3 film was deposited on top of SRO layer. The RHEED pattern changed from streaky to 3 D spot after 2 nm CaTiO_3 film, which means island growth on the film surface.

AFM micrographs of the surface morphology before deposition and after deposition 30 nm CaTiO_3 thin film with electrode in the middle are depicted in Figure 4-11. It is clearly shown the high roughness of the film with an island height of 5 nm, while

blurred step can be recognized as well. Since SrRuO_3 layer is fully relax during growing, less roughness of the film is obtained than the one without SrRuO_3 bottom layer.

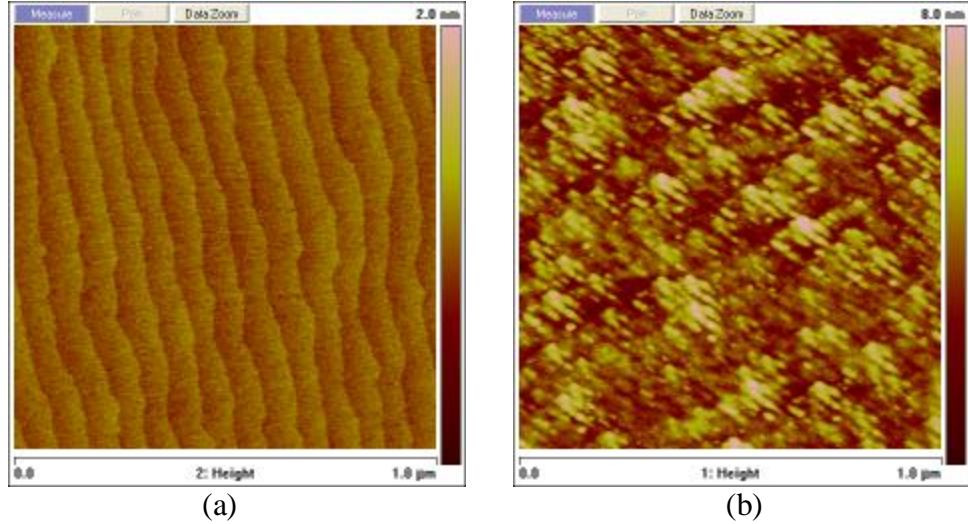
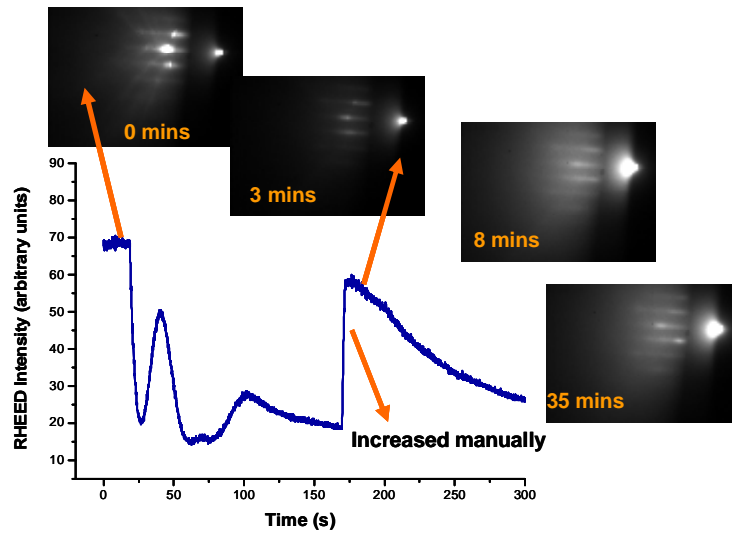


Figure 4-11 AFM micrographs (a) before deposition (b) after deposition CaTiO_3 on LaAlO_3 substrates at 750°C with 30 nm SrRuO_3 electrode in the middle.

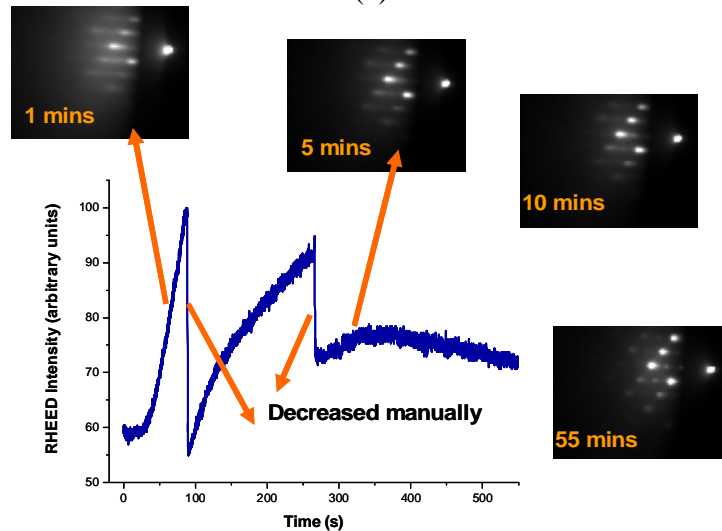
After characterization of this film, a top electrode (SrRuO_3) was grown with shadow mask [17] in order to measure electric properties later on. The deposition conditions are shown in 4.1.

4.4.2 Growth studies of CaRuO_3 on LaAlO_3

Another material CaRuO_3 was also used as bottom and top electrode, the misfit of $\text{CaRuO}_3//\text{LaAlO}_3$ (1.55%) is much smaller than that of $\text{SrRuO}_3//\text{LaAlO}_3$ (3.56%). Typical RHEED data of the CaRuO_3 growth and CaTiO_3 growth are shown in Figure 4-12. The parameters for CaRuO_3 deposition are the same as for SrRuO_3 . The RHEED intensity starts with a sharp oscillation and a period of 20 pulses. After that, a large drop in RHEED intensity is observed. The first inset of Figure 4-12(a) is the RHEED pattern after LaAlO_3 buffer layer has been grown, which indicates the surface morphology before CaRuO_3 growth. The sharp and bright spot shows a substrate that is highly crystalline. From the RHEED pattern taken at different thickness of 2 nm, 5 nm and 22 nm, a streaky pattern is observed without become 3 D patterns in the middle. In this case, the growth follows a typical step flow mechanism, which indicates a flat and smooth surface.



(a)



(b)

Figure 4-12 RHEED intensity of $\text{CaRuO}_3/\text{LaAlO}_3$ multilayer growth on LaAlO_3 substrate. (a) CaRuO_3 film growth. (b) CaTiO_3 film growth. Inset is the RHEED pattern before, during and after deposition.

After growing a 30nm CaRuO_3 bottom electrode, CaTiO_3 was grown on top of CaRuO_3 , see Figure 4-12 (b). The RHEED monitoring displays an increase in intensity, while the RHEED pattern changes from 2 D to 3 D in the first 5 minutes. It indicates a roughened surface morphology of CaTiO_3 film.

Top CaRuO_3 electrode was grown with shadow mask for further electric measurement. The growth condition was mentioned in 4.1.

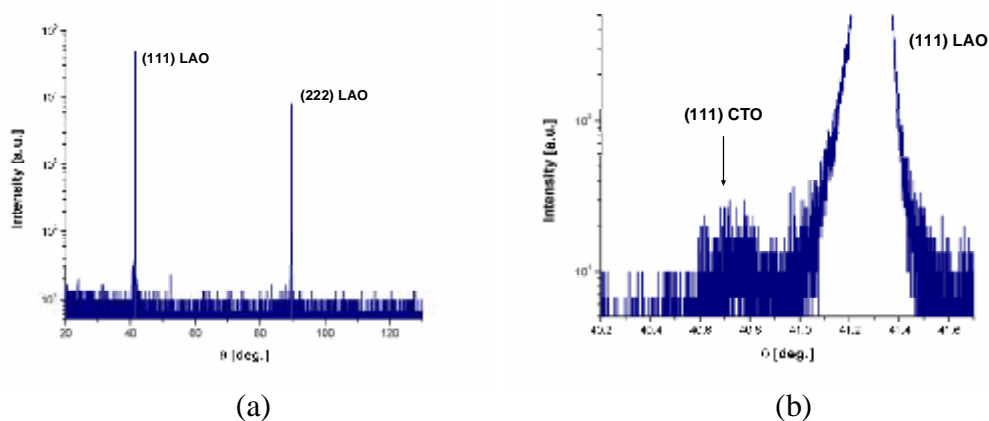
Chapter 5. Results and discussion

In this chapter, the presented results will be discussed, by showing the structure of films grown in different conditions. From the XRD measurement, fully strained CaTiO_3 thin film is proved. Further electric measurement, shows no signs of ferroelectric properties at room temperature.

5.1 Structural properties

Coherent growth of CaTiO_3 thin films on single crystal (111) LaAlO_3 substrates will induce compressive strain when grown. The in-plane misfit between LaAlO_3 and CaTiO_3 is 0.79%. The initial growth and surface roughness has been shown in Figure 4-4 and 4-5.

The crystallinity of this thin film is investigated by X-ray diffraction. A θ - 2θ scan for a 50 nm CaTiO_3 thin film grown on (111) LaAlO_3 substrate is shown on Figure 5-1 (a). Only the (111) peaks from LaAlO_3 substrate and CaTiO_3 film are present, which indicate a c-axis growth. The peak around 40.72° , shown in Figure 5-1 (b), is attributed as CaTiO_3 film. Figure 5-1 (c) shows the ϕ scan of the same sample around (110) peak. Sharp peaks appear at the ϕ angle with 120° interval, suggesting a three-fold symmetric crystal. Twins structure can be obtained from the zoom in peak, see Figure 5-1 (d). Meanwhile, an excellent alignments through (110) direction between the LaAlO_3 substrate and CaTiO_3 film is displayed.



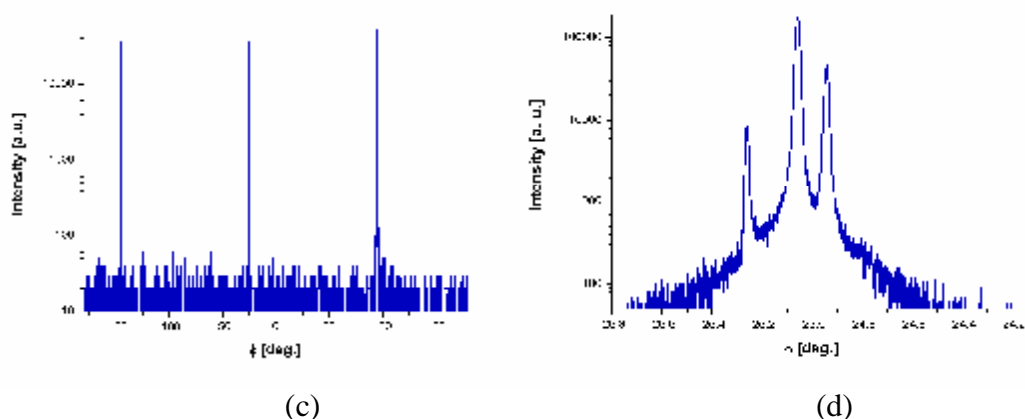


Figure 5-1 X-ray diffraction spectra for a 50 nm CaTiO_3 film on a (111) LaAlO_3 substrate. (a) θ - 2θ scan, and (b) zoom in scan of (a) from 40.2° to 41.6° with a clear film out-of-plane peak and (c) Φ scans around (110) orientation. (d) idem of (c) from -25.8° to -24.2° . It indicates a clear three-fold symmetry and twins structure on the surface.

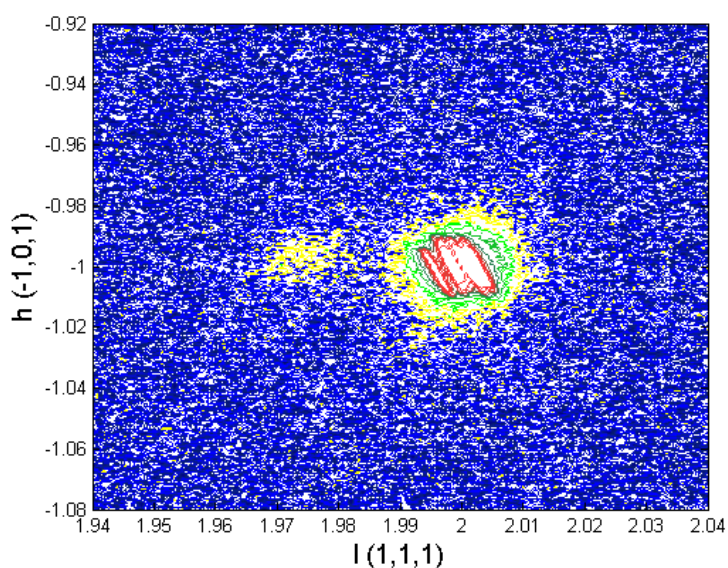


Figure 5-2 HL scan around (321) reflection of CaTiO_3 film on LaAlO_3 substrates without LaAlO_3 buffer layers. The H values of both the film and substrate are the same.

Figure 5-2 gives the HL reciprocal space map around (321) reflections of the same 50nm thick LaAlO_3 sample. Since the CaTiO_3 film and LaAlO_3 substrates are in special orientation (111), L (111) is chosen as the out-of-plane vector in reciprocal map and H (-1,0,1) is chosen as the in-plane vector. The Figure shows that besides the substrate peak, there is a peak from CaTiO_3 film. The peaks of LaAlO_3 substrate and CaTiO_3 film have identical h (-1,0,1) values, with a slightly different l (1,1,1) values. From this result, it can be concluded that the in-plane film lattice is matched well with the substrate, while CaTiO_3 film has a larger out-of-plane value than

LaAlO₃ substrate. The CaTiO₃ film was coherently grown with a (111) orientation with strain state.

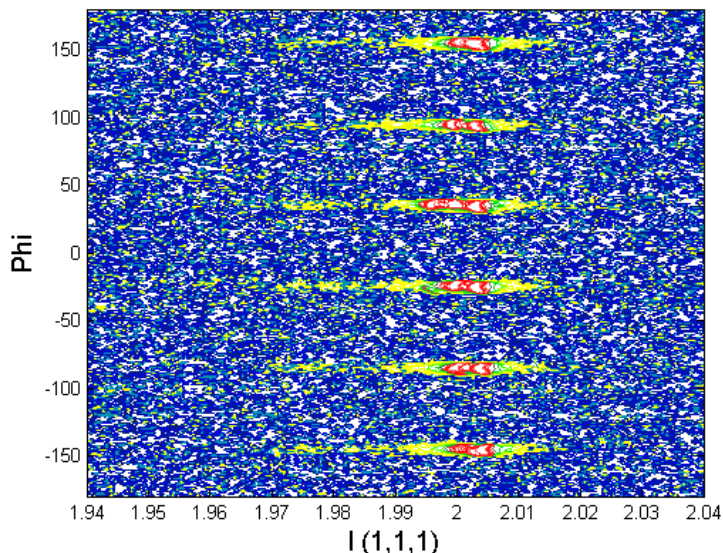


Figure 5-3 L-Phi scan around (321) reflection of CaTiO₃ film on LaAlO₃ substrate buffered LaAlO₃ layer. A six folder symmetry structure can be aligned from different φ angle.

In order to get an in-plane alignment, an φ -L scan was taken around the (321) reflection of CaTiO₃ film on LaAlO₃ substrate buffered LaAlO₃ layer, see Figure 5-3. L (111) is the reciprocal vector around (321) spot in reciprocal space map. H (-1,0,1) was fixed as -1. And an φ scan was used from -180° to 180°. From Figure 5-3, six main peaks are obtained as substrate peaks, which split up into two in the centre. Six small peaks at 1.975 L value are attributed as CaTiO₃ film peaks. It is indicated a six-fold symmetry from (111) orientation and a well-aligned sample. In order to do a reciprocal map, one of the six peaks is chosen. Then a reciprocal map can be set around one of the reachable spot in the map, see Figure 2-4.

The reciprocal map of CaTiO₃ film on LaAlO₃ substrate with a LaAlO₃ buffer layer is shown in Figure 5-4. HL scan around (321) reflection and (420) reflection of this sample are shown. Both plots show same H (-1,0,1) value for the substrate peak and the film peak, with a slight smaller L (111) values of CaTiO₃ film. The L value in reciprocal space is displayed as 1.975 in both maps. In reciprocal space, a small L value means a large d value in real space. Since the lattice mismatch of film and substrate is 0.79%, the non-strain CaTiO₃ film correspond to be 1.984 for L (111) value from the calculation of the proportion of two different lattice constant. However, it shows an L value 1.975 for CaTiO₃ film in reciprocal map. It is clear that there is an elongation in out-of-plane direction, while the in-plane lattice is fully strain. The main two peaks in the middle of substrate is cause by twin structure.

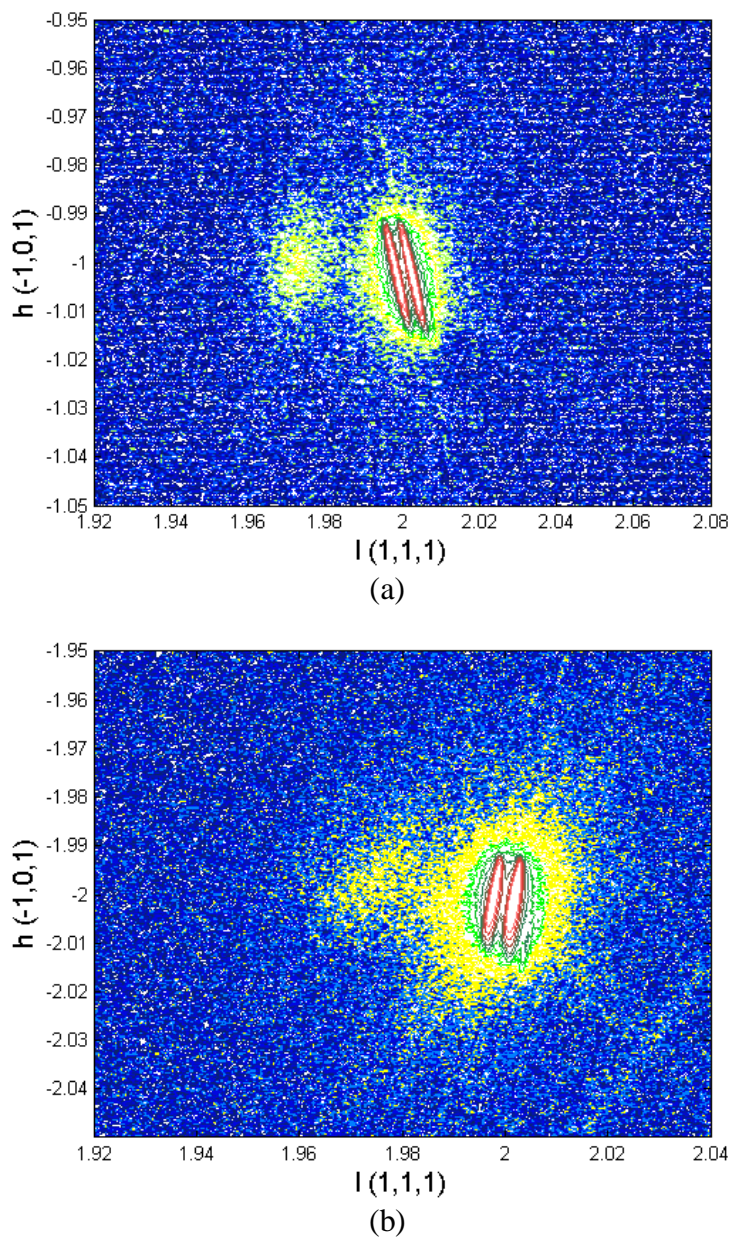


Figure 5-4 (a) HL scan around (321) reflection of CaTiO_3 film on LaAlO_3 substrates with LaAlO_3 buffer layer. (b) HL scan around (420) reflection of CaTiO_3 film on LaAlO_3 substrates with LaAlO_3 buffer layers. Both two reciprocal space maps show the same H values from the film and substrate.

Another reciprocal map is shown about HL scan around (321) reflection of CaTiO_3 film on LaAlO_3 substrates with SrRuO_3 bottom electrode, in Figure 5-5. The additional peak is attributed to the film peak. In this case, both H (-1,0,1) and L (1,1,1) direction show a big misfit from substrate and films. The growth with SRO electrode does not give a strained film. It is probably due to the big mismatch between LaAlO_3 and SrRuO_3 .

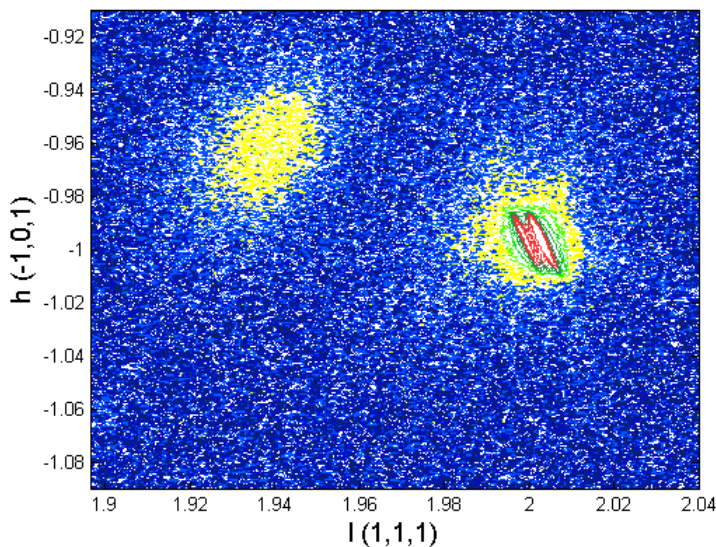


Figure 5-5 HL scan around (321) reflection of CaTiO_3 film on LaAlO_3 substrates with SrRuO_3 bottom electrode. The film peak is not identical with the LaAlO_3 substrate in both H direction and L direction, which indicates the film is relax during growing.

The CaRuO_3 electrode growth structure is shown in Figure 5-6, which shown HL scan around (321) reflection of CaTiO_3 and CaRuO_3 film on LaAlO_3 substrate. The film peak is shown around 1.975 in L (111) direction, with the same values in H (-1,0,1). Meanwhile, a small peak exists beforehand, with a 1.952 L value and -1 H value, which is indicated the CaTiO_3 film peak with 20 nm thick of this sample. From this reciprocal space map, it was estimated that the in-plane lattice parameters of $\text{CaRuO}_3/\text{LaAlO}_3$ film are equal to that of LaAlO_3 . It confirms the full strain growth of CaTiO_3 film with bottom electrode on (111) LaAlO_3 substrate was obtained.

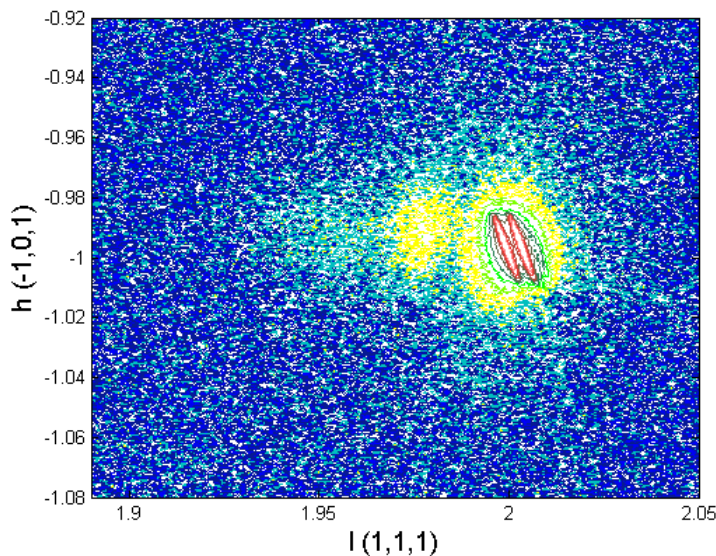


Figure 5-6 HL scan around (321) reflection of CaTiO_3 film on LaAlO_3 substrates with CaRuO_3 bottom electrode. Both CaRuO_3 film and CaTiO_3 film shows the same H value as LaAlO_3 substrate.

5.2 Electric properties

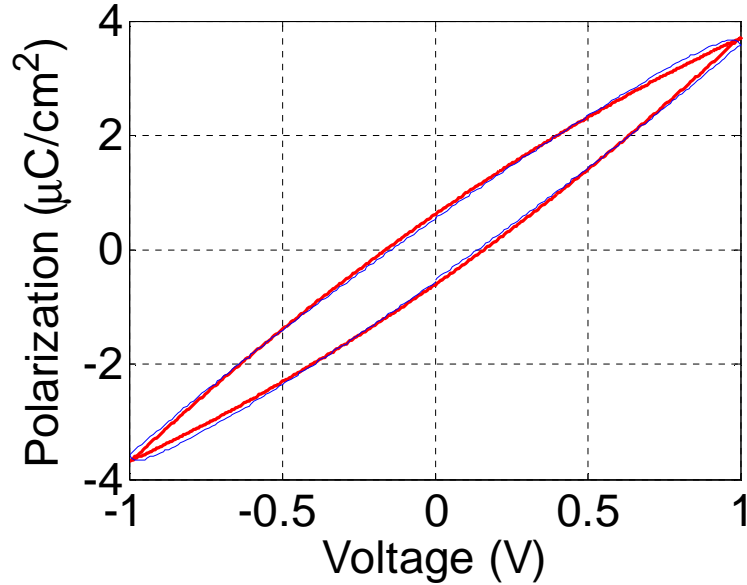


Figure 5-7. Polarisation-Electric field (PE) curve of 50nm CaTiO_3 thin film. The resistivity is $67 \text{ M}\Omega\cdot\text{m}$ and the capacitance is 0.37nF .

It has been shown that $\text{CaRuO}_3//\text{CaTiO}_3$ can be grown fully strain on (111) LaAlO_3 , see Figure 5-6. Therefore it is possible to do electric measurement after grow electrode with stencil on top of the thin film. In this case, electric properties can be measured by approaching two top electrodes. Polarisation-Electric field (PE) curve of 50 nm CaTiO_3 thin film with electrode CaRuO_3 is shown in Figure 5-7. The different between this loop and hysteresis loop (see figure 1-2) indicates that no signs of ferroelectricity at room temperature are obtained from this measurement. The capacitance is calculated as 0.37nF , while the resistivity is $67 \text{ M}\Omega\cdot\text{m}$. From this data, a dielectric constant can be calculated from equation.

$$C = \frac{d}{A \times \epsilon_0 \times \epsilon_r} \quad (5.1)$$

The dielectric constant of CaTiO_3 was calculated as 105, which is comparable to literature [18].

Chapter 6 Conclusions and recommendations

6.1 Conclusions

- (111) LaAlO_3 substrates surfaces with single termination and smooth step edges were achieved.
- CaTiO_3 was grown with in-plane strain on the LaAlO_3 substrates.
- A CaRuO_3 bottom electrode with a CaTiO_3 film was grown strained on LaAlO_3 substrates.
- The $\text{CaRuO}_3//\text{CaTiO}_3//\text{CaRuO}_3$ was shown to have a similar capacitance to previous experiments.
- The $\text{CaRuO}_3//\text{CaTiO}_3//\text{CaRuO}_3$ do not show signs of ferroelectricity at room temperature.

The epitaxial growth of calcium titanate thin film along (111) direction by pulsed laser deposition was studied. With the full treated LaAlO_3 substrates, CaTiO_3 will be strained in (111) direction by epitaxial growth, which is the same orientation from the calculation [6].

For the surface treatment, selective removal of alumina layer was achieved by an alkaline treatment and followed by annealing in O_2 flow. The result surface morphology was studied by AFM. CaTiO_3 thin films were epitaxially grown on (111) oriented LaAlO_3 substrates (with or without a LaAlO_3 buffer layer) by PLD. RHEED and AFM were used to analyze the growth mode and surface morphology, while X-ray diffraction and HREM were exploited for structure characterization of the thin films. The XRD reciprocal map showed that the films were coherent growth, with complete in plane crystalline alignment with substrates, which agree with the image from HRTEM. The LaAlO_3 buffer layer is shown to improve the surface morphology of the LaAlO_3 substrates.

In order to measure the ferroelectric loop, different electrodes (SrRuO_3 , CaRuO_3) were grown as the bottom layer and top layer by PLD (with LaAlO_3 or SrTiO_3 buffer layer on LaAlO_3 substrates). From the AFM data, CaTiO_3 film with SrRuO_3 bottom electrode gives better morphology and less roughness compare with the one without bottom electrode. XRD date provides that the film with SrRuO_3 was full relaxed on the LaAlO_3 substrates. In reciprocal map, the film peak in not alignment with substrate peak in both in plane orientation and out plane orientation. The results of CaTiO_3 thin film with CaRuO_3 bottom electrode show high quality epitaxial growth on (111) LaAlO_3 substrates by PLD. From the reciprocal space map, both CaRuO_3 and CaTiO_3 films are found fully stain on the substrates.

6.2 Recommendations

The discussion in this thesis has shown that (111) CaTiO_3 thin films were coherently grown on (111) LaAlO_3 substrates. Both XRD and TEM results indicate it is fully strain on LaAlO_3 substrate. As described from the first principle calculation, the ferroelectric phase of CaTiO_3 may be possible to be stabilized. However, electric measurement did not show a hysteresis loop of the PE curve at room temperature. In order to simplify the picture, the simulation uses a temperature of 0 K. It may be the reason no ferroelectricity was observed in CaTiO_3 at room temperature. Therefore, it would be interesting to try more electric measurements at low temperature.

In addition, more High-resolution TEM will be useful to study the interface of film growth, which includes both initial CaTiO_3 film growth and CaRuO_3 electrode growth. By means of analysis the misfit and dislocation in the interface, growth conditions can be optimized to get a better coherent growth.

References

- [1] M.E. Lines and A.M. Glass, Principles and Applications of Ferroelectric and Related Materials, Clarendon Press, Oxford (1997)
- [2] V.V. Lemanov, A.V. Sotnikov, E.P. Sminova, M. Weihnacht, R. Kunze, *Solid State Commun.* **110**, 611 (1999).
- [3] B.J. Kenndey, C.J. Howard, B.C. Chakoumakos, *Phys. Rev. B* **59**, 4023 (1999).
- [4] B.J. Kenndey, C.J. Howard, B.C. Chakoumakos, *J. Phys. Condens. Matter.* **11**, 1479 (1999).
- [5] Y.X. Wang, *Solid State Commun.* **117**, 461 (2001).
- [6] C.J. Eklund, in preparation, (2007).
- [7] W. Zhong, D. Vanderbilt, *Phys. Lett.* **74**, 2587 (1995).
- [8] O.I. Lebedev, G. Van Tendeloo, S. Amelinckx, H.L. Ju, K.M. Krishnan, *Phil. Mag.* **A80**, 673 (2000).
- [9] A.K. Adak, P. Pramanik, *Mater. Lett.* **30**, 269 (1997).
- [10] P. Peschev, V. Slavova, *Mater. Res. Bull.* **29**, 255 (1994).
- [11] Z.L. Wang, *Surf. Sci.* **328**, 141 (1995).
- [12] C.H. Kim, *Mater. Res. Bull.* **36**, 1561 (2001).
- [13] S.A. Hayward, F.D. Morrison, *Phys. Rev. B* **72** (2005) 054110.
- [14] Picture was taken from interface engineering for oxide electronics, by M. Huijben.
- [15] G. Rijnders. The initial growth of complex oxide: study and manipulation. Ph.D. thesis (2001)
- [16] A. Brinkman, M. Huijben, M. van Zalk, J. Huijben, U. Zeitler, J.C. Maan, W.G. van der Wiel, G. Rijnders, D.H.A. Blank, H. Hilgenkamp, *Nature Mater.*, **6** 493 (2007).
- [17] P.T. Riele, A. Janssens, *J. Phys. Conference Series* **59**, 404 (2007).
- [18] B.D. Lee, H.R. Lee, *Ceram. Int.* **31**, 143 (2005).

